AN EXPERIMENTAL INVESTIGATION
OF THREE BALLOON-TYPE ENCLOSURES
FOR THERMAL CONTROL OF SATELLITES

by George E. Sweet

Langley Research Center
Hampton, Va. 23365

0133041

1. Report No. NASA TN D-6224	2. Government Accession No.	3. Recipient's Catalog No.
4. Title and Subtitle AN EXPERIMENTAL INVESTIGATION OF THREE BALLOON-TYPE ENCLOSURES FOR THERMAL CONTROL OF SATELLITES		5. Report Date June 1971
		6. Performing Organization Code
7. Author(s) George E. Sweet		8. Performing Organization Report No. L-7015
		10. Work Unit No. 124-09-26-03
9. Performing Organization Name and Address NASA Langley Research Center Hampton, Va. 23365		11. Contract or Grant No.
		13. Type of Report and Period Covered Technical Note
12. Sponsoring Agency Name and Address National Aeronautics and Space Administration Washington, D.C. 20546		14. Sponsoring Agency Code

15. Supplementary Notes

16. Abstract

Thermal-vacuum tests of three balloon-type thermal-control enclosures for satellites indicate that payload temperature uniformity for these designs would be one to two orders of magnitude better than that for an unshielded satellite. Results indicate that temperature uniformities of 5° to 10° K are feasible for a small, solid, nonconducting payload located near the center of the enclosure. Measured results indicate that the temperature uniformity of surfaces near the center of the enclosure is relatively insensitive to satellite orientation, changes in payload heat dissipation, and the presence of an enclosure viewport opening. Balloon interiors of high reflectance provided the most uniform temperatures for an enclosed payload and the least uniform balloon temperatures.

17. Key Words (Suggested by Author(s)) Satellite Thermal control Orbiting telescope	18. Distribution Statement Unclassified – Unlimited		
19. Security Classif. (of this report) Unclassified	20. Security Classif. (of this page) Unclassified	21. No. of Pages 46	22. Price* $3.00

*For sale by the National Technical Information Service, Springfield, Virginia 22151

AN EXPERIMENTAL INVESTIGATION
OF THREE BALLOON-TYPE ENCLOSURES FOR
THERMAL CONTROL OF SATELLITES

By George E. Sweet
Langley Research Center

SUMMARY

Thermal-vacuum tests of three balloon-type thermal-control enclosures for satellites indicate that payload temperature uniformity for these shielded satellites would be one to two orders of magnitude better than that for an unshielded satellite. Results indicate that temperature uniformities of 5° to 10° K are feasible for a small, solid, nonconducting payload located near the center of the enclosure. Measured results indicate that the temperature uniformity of surfaces near the center of the enclosure is relatively insensitive to satellite orientation, changes in payload heat dissipation, and the presence of an enclosure viewport opening. Balloon interiors of high reflectance provided the most uniform temperatures for an enclosed payload and the least uniform balloon temperatures.

INTRODUCTION

Reference 1 suggested that a balloon enclosure would provide a uniform thermal environment for an orbiting telescope. Because this enclosure is spherical, the telescope temperatures would be relatively insensitive to orientation. Multiple reflections by the interior walls would provide relatively uniform irradiances and temperatures at the surfaces of the enclosed telescope. For manned spacecraft near the earth, enclosures would also provide uniform lighting and a near-room-temperature environment for astronauts performing assembly and/or repair functions.

The enclosure-thermal-control technique could be applied to a satellite that required uniform temperatures. Reference 2 demonstrated the thermal advantages of this concept and discussed one type of space deployable structure. The technology for designing and constructing deployable structures is included in references 3, 4, and 5. This report is an extension of reference 2 and presents more details on thermal models of the Echo II, modified Echo II, and polka-dot balloon enclosures. Included are experimental and analytical results that indicate the effects of internal heating and enclosure openings on the temperatures of payloads that are small as compared to the enclosure.

SYMBOLS

A	area, centimeters^2
ΔA	surface area used in view-factor calculation
E	incident energy per unit area, watts per centimeter^2
F	view factor
H	total irradiance at radiometer, watts per centimeter^2
Q	rate of heat dissipation by payload, watts
Q_{vp}	rate of balloon heat dissipation through viewport, watts
r	balloon radius, centimeters
r_{vp}	viewport radius, centimeters
T	temperature, $^{\circ}$K
T_e	equivalent black-body temperature of heat sources, $\left(\dfrac{H}{\sigma}\right)^{1/4}$, $^{\circ}$K
ΔT_e	temperature uniformity $\left(T_{e,H} - T_{e,C}\right)$, $^{\circ}$K
X,Y,Z	balloon axes
α	absorptance
β,δ	angles defining surface element used in calculating view factor, degrees (see fig. 24)
ϵ	emittance
θ,ϕ	coordinates for a unit radius sphere, degrees
ρ	reflectance

2

σ Stefan-Boltzmann constant, 5.67×10^{-12} watt-centimeter^{-2}-$^{\circ}$K^{-4}

λ wavelength, micrometers

χ_1, χ_2 angles between normal to a surface and a directed line, degrees (fig. 24)

ω solid angle, steradians

Subscripts:

ΔA referenced to surface area used in view-factor calculations

C   cold side

H   hot side

i   inside

n   index associated with number of surface elements

o   outside

s   solar

sc   spherical cap

θ, ϕ associated with sphere coordinates

APPARATUS

Thermal-vacuum tests of the balloon enclosures were conducted at the Langley Research Center in the 5-foot-diameter by 10-foot-long vacuum chamber, in which a carbon-arc searchlight was used as a solar simulator. Figure 1 shows the arrangement of the test apparatus which is described in reference 6.

Model Support

Figure 2 shows a balloon model mounted on the support apparatus as installed in the vacuum chamber. The models were reinforced at their poles (a fiber-glass annulus at one pole and a grommet at the other pole) for mounting to the instrumentation bar

shown in figure 3. The model support was motor-driven so that balloon skin temperatures and equivalent black-body temperatures along the balloon diameter could be measured at different positions with respect to the solar simulator. The model was positioned to an accuracy of $\pm 3^{\mathrm{o}}$.

<div align="center">Balloon Models</div>

Three scale model balloons, each 50.8 centimeters in diameter, were tested. These scale models represented the Echo II, modified Echo II, and typical polka-dot balloon structures. The construction materials and their optical properties are summarized in table I.

<div align="center">TABLE I.- SUMMARY OF PROPERTIES OF SCALE MODEL BALLOONS</div>

Balloon	Echo II		Modified Echo II		Polka dot	
	Inside	Outside	Inside	Outside	Inside	Outside
Material	Sandwich thickness of 0.0046 mm aluminum, 0.0088 mm Mylar, and 0.0046 mm aluminum		Mylar 0.0127 mm	Same as Echo II sandwich	Same as Echo II sandwich	Mylar 0.0127 mm
Coating	India ink	Alodine 401-45 (0.2 mg/cm2)	Vapor-deposited aluminum	Alodine 401-45 (0.2 mg/cm2)	Alodine 401-45 (0.2 mg/cm2)	91-percent vapor-deposited aluminum, 9-percent white paint
α_s	-------	0.28	----------------	0.28	--------------	0.14
ϵ_0	0.60	0.17	0.04	0.17	0.17	0.12
α_s/ϵ_0	------	1.60	----------------	1.60	--------------	1.15

These materials were rigid enough to maintain a spherical shape, without pressurization, after an initial inflation. Several vent holes, 0.5 centimeter in diameter, and leakage around the instrumentation leads allowed the balloon pressure to come to equilibrium with the vacuum chamber.

Echo II model.- The Echo II scale model was constructed from gore samples removed from Echo II balloons. The optical properties for this model were determined from the arithmetic average of 20 reflectance measurements. The solar absorptance α_s ranged from 0.24 to 0.31 and the low-temperature emittance ϵ from 0.16 to 0.19. The average ratio of solar absorptance to low-temperature emittance α_s/ϵ was 1.60 as compared with 1.84 for the laboratory-prepared samples reported in reference 7.

Modified Echo II model.- The modified Echo II balloon model was constructed by laminating Echo II gore samples to aluminized Mylar (polyethylene terephthalate). The aluminized surface faced toward the inside of the balloon. The emittance of this surface was determined to be 0.04 from calorimetric measurements by using the apparatus described in reference 7. The purposes of the highly reflective interior was to increase the irradiance uniformity near the center of the balloon by increasing the number of multiple reflections.

Polka-dot balloon.- The polka-dot balloon model was designed to provide a near-room-temperature environment and uniform temperatures over the surfaces of a small payload located near the center of the balloon. Consideration was also given to maintaining skin temperatures below those that might melt or shrink balloon plastics. Equations presented in reference 2 were employed in this design.

This balloon was constructed by laminating Echo II gore samples to aluminized plastic. The aluminized surface faced the outside and an Alodine coated surface faced inside. Dots of white paint (zinc-oxide pigmented silicone elastomer) were applied uniformly to 9 percent of the balloon surface to reduce the balloon temperature. As reported in reference 8, the paint had a solar absorptance of 0.22 and a low-temperature emittance of 0.87. Reflectance measurements indicated that the solar absorptance of the aluminized Mylar was 0.13 and the low-temperature emittance was 0.04.

Instrumentation

Radiometers were used to measure the energy incident to the balloon walls and equivalent black-body temperatures of irradiance along the balloon diameter. These radiometers are fully described in reference 9. Figure 3 shows a photograph of these radiometers mounted on the instrumentation bar at the locations shown in figure 4. In this study the black-body temperatures T_e of the radiometers mounted on the instrument bar are interpreted as the temperature distribution that would occur in a slender payload, having a nonconducting skin, that absorbed and emitted radiation only from its outside surface. Thus, the temperatures presented are indicative of the maximum temperature variations that would occur at the outside surface of a highly insulated spacecraft, for which the outside surfaces had gray optical properties. (See ref. 2.)

One grid-type thermocouple made from 25.4-micrometer (1-mil) chromel-alumel wire was sandwiched between skin laminations of each balloon to measure the average skin temperature. The location of this thermocouple is shown in figure 4. The model was rotated with respect to the simulator to obtain temperature distributions. Temperatures were measured with strip-chart recorders with an accuracy of ±2° K for the skin thermocouple and ±4° K for the radiometers.

Solar-Simulator Irradiance

Initial uniformity surveys indicated unacceptably large variations (0.5 to 1.6 solar constants) in the simulator radiance. This uniformity was improved by increasing the overall simulator intensity and attentuating the hot areas with screens. The screen pattern used (see fig. 5) was located outside the vacuum chamber as shown in figure 1. Contours of constant irradiance at the survey plane are shown in figure 6. These contours were determined from cross plots of 217 radiometer readings. The radiometers were 1.3 centimeters in diameter. Tests were conducted at an average irradiance of 1.03 solar constants to correct for differences between sun and carbon-arc spectrums. (See ref. 10.) Average irradiances were maintained within ±5 percent of 1.03 solar constants with the aid of the solar-simulator radiometer located as shown in figure 1. Figure 6, however, shows that the excursions from these averages were rather large.

TESTS

All tests were conducted at chamber pressures less than 1×10^{-5} torr (1.333 millinewtons/meter^2). Preliminary tests indicated that 1/2 hour was required for the balloon pressure to come to equilibrium. Two hours were allowed before starting the tests to insure that convection was insignificant. No attempt was made to simulate albedo or earth-emitted heat, and data were recorded only after the models came to temperature equilibrium.

RESULTS AND DISCUSSION

Measured Results

Skin temperatures T and equivalent black-body temperatures T_e along the balloon diameters were measured for all models. Both the polka-dot and the Echo II models maintained a spherical shape during the testing. Small wrinkles formed at the subsolar point of the modified Echo II model as it was rotated in the solar simulator beam. This wrinkling was caused by heat shrinkage of plastic in the skin laminations. The distortions increased with exposure time and became severe when solar simulator heat entered the viewport. (See fig. 7.) It is believed that results from skin temperature and viewport-open tests were not significantly affected since only a small portion of the balloon had become wrinkled. The data taken after the wrinkling was noticed are included only to show general temperature trends.

Skin temperatures.- The solar simulator irradiance along the skin temperature traverses is shown in figure 6. Figure 8 presents a comparison of the skin temperatures

6

for the test models and shows that the Echo II skin temperatures are the most uniform. This uniformity occurs because the high emittance interior allowed a rapid dissipation of heat from the hot areas.

The Echo II model skin thickness was not scaled. Thus, heat conduction along the skin was too large in proportion to the inverse of the scale factor, 81:1. References 11 and 12 suggest that the disproportionately thick model skin should not have affected the Echo II model temperatures by more than 4 percent.

Because of the thick skin of this model, temperature variations on the polka-dot balloon model, between the white and aluminized areas, are not representative of those on a larger-scale balloon. Measurements were made to determine the maximum possible skin temperature. This maximum value would occur in the aluminized areas if the dots were widely spaced. This condition was simulated by removing the white paint in a 5-centimeter-diameter circle around the thermocouple and cutting insulating gaps to minimize heat conduction between this circle and the rest of the balloon.

Internal temperatures along a balloon diameter.- Internal temperatures T_e and temperature differences ΔT_e along the balloon axis for the three test models were measured for varying orientations of the model with respect to the solar simulator for the following conditions:

Viewport closed, payload heaters operating
Viewport closed, payload heaters off
Viewport open, payload heaters operating
Viewport open, payload heaters off

Results for the Echo II model are presented in figures 9 to 11; those for the modified Echo II are in figures 12 and 13; and those for the polka-dot model, in figures 14 to 17. These temperature trends are indicative of the maximum temperature gradients that would occur in a slender, nonconducting payload such as a telescope. These temperatures are several orders of magnitude more uniform than for a similar payload that was not enclosed. (See ref. 2.)

Figure 18 presents a comparison of the temperature uniformity ΔT_e for the three models. The modified Echo II model provided the most uniform internal temperatures. This uniformity was relatively insensitive to model orientation. The temperature uniformity at the center of the models $(\theta = 90^O)$ was 4° K for the modified Echo II, 6° K for the polka-dot model, and 20° K for the Echo II. Figure 18 also shows that the temperature uniformity of the modified Echo II and polka-dot balloon decreased near the balloon walls. These results suggest that a payload that requires good temperature uniformity should be centrally located and perhaps only 50 to 60 percent of the balloon diameter in length.

Effects of viewport and payload heating on internal temperatures.- Because balloon enclosures provide passive thermal control, consideration should be given to the effects of payload heating and viewport heat loss on payload temperatures. Figure 9 shows that temperature levels T_e for the Echo II model are relatively insensitive to the simulated payload heating and the viewport heat loss. Figure 12, on the other hand, shows that this heat increased the temperature levels within the modified Echo II model by about 15° K. This temperature rise is attributable to the "thermos bottle" effect of the reflective interior ($\rho = 0.96$). This temperature sensitivity is actually rather small when the magnitude of the model heating is considered. For example, the corresponding payload heat dissipated within a 20-meter-diameter balloon would be $(4.64$ W$) \times$ (Scale factor)^2 or about 7.3 kW. (See ref. 12.) This amount is at least an order of magnitude greater than that of most satellites. For a 20-meter-diameter enclosure with the same optical properties as the modified Echo II, the payload-temperature sensitivity to heating would be 15° K/7.3 kW or about 2^O K/kW. Thus, the present results suggest that payload temperature levels are relatively insensitive to changes in payload heating for low-reflectance interiors and are moderately sensitive for high-reflectance interiors. An examination of the expression for balloon internal energy E_i (see eq. (A3) in appendix A) suggests that this insensitivity is due to the large area over which the heat dissipated; that is, the balloon surface is an effective radiator.

The primary effect of the Echo II viewport was to lower the temperatures near the opening as shown in figure 8. Because of the greater number of multiple reflections within the other two models when the viewport was open, the temperatures remained relatively uniform but reduced in level. (See figs. 12 and 14.) The calculated total heat leaving through the viewport (eq. (A5)) from a point heat source at the center of the balloon is summarized in the following table:

	$Q_{vp} = A_{sc}\left(E_i + \dfrac{Q}{4\pi r^2}\right)$, watts		
	Echo II	Modified Echo II	Polka-dot
Heaters off	4.43	3.63	2.93
Heaters on (4.64 watts)	4.76	4.74	3.50

The calculated internal heat loss through the viewport, $\left[\dfrac{\left(Q_{vp}\right)_{\text{heat on}} - \left(Q_{vp}\right)_{\text{heat off}}}{Q = 4.64 \text{ watts}}\right] \times 100$, was 7.1 percent for the Echo II ($\rho = 0.40$), 24 percent for the modified Echo II ($\rho = 0.96$), and 12.4 percent for the polka-dot model ($\rho = 0.83$). These calculations suggest that a

viewport is a more effective method of dissipating payload heat when the interior reflectance is high.

Figures 11, 16, and 17 show the effect of simulator heat entering the viewports on the internal temperatures of the Echo II and polka-dot balloons. The relatively absorptive interior surface of the Echo II caused the radiometers adjacent to the viewport to become warm. Figure 16 shows that when the interior surface was specular, the radiometers farthest from the viewport were the warmest for the polka-dot model. This result was caused by specular reflections as indicated in the following sketch:
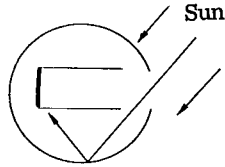
These reflections caused the normally cold internal temperatures to become the warmest as the model was oriented to allow more radiation to enter the viewport. (See fig. 17.)

Comparison of Measured and Calculated Results

Balloon α_s/ϵ_o ratios.- Reference 2, for example, shows that the energy incident to the inside wall of a spherical shell is independent of the distribution of external heating. This energy E_i was determined experimentally from temperatures T_e measured with radiometers attached to the inside surfaces of the balloons. Experimental α_s/ϵ_o ratios were determined from these values of E_i by writing equation (A4), Appendix A, as

$$\frac{\alpha_s}{\epsilon_o} = \frac{4E_i}{E_s}\left[1 + \frac{A_{sc}}{4\pi r^2}\left(\frac{1}{\epsilon_o} + \frac{1}{\epsilon_i} - 1\right)\right] \tag{1}$$

where E_i is σT_e^4. Experimental α_s/ϵ_o ratios are compared with ratios determined from reflectance and calorimetric measurements of similar balloon materials in the following table:

Model	α_s/ϵ_o from standard laboratory techniques	α_s/ϵ_o from model test measurements	
		Viewport closed	Viewport open
Echo II	1.60	1.58	1.55
Modified Echo II	1.60	1.86	1.65
Polka-dot	1.15	1.12	1.09

The discrepancy between model test measurements and those obtained by standard laboratory techniques for the modified Echo II balloon with the viewport closed was probably caused by the large number of wrinkles that had accumulated at the time of this test. The purpose of the comparison in this table was to show the applicability of published optical properties to thermal balance calculations. This effort was only partly successful because of conflicting published and unpublished results. For example, the α_s/ϵ_o ratio of the Echo II material as determined from an average of a large number of samples was 1.60 as compared to 1.84 reported in reference 7. The balloon material optical-property data are given in references 7 and 8.

Because of differences in reported optical properties, it is recommended that thermal-balance predictions be verified by tests of spacecraft and/or thermal models in a simulated space environment.

Balloon skin temperatures.- Figure 19 compares measured and calculated skin temperatures. Calculated temperatures were determined from the following expression given in reference 2:

$$T_{\Delta A} = \left[\frac{1}{\sigma(\epsilon_i + \epsilon_o)}(\alpha_s E_s \cos\theta + \epsilon_i E_i)\right]^{1/4} \tag{2}$$

where θ is the angle formed between the solar vector and the normal to a small balloon area ΔA. For $90^o < \theta < 270^o$, the skin temperature is constant and E_s is taken as zero. As previously noted, the measured temperatures for the polka-dot balloon are representative of the maximum expected temperatures in the aluminized plastic areas; that is, conductive heat transfer between the aluminized area containing the thermocouple and the rest of the balloon was minimized. Two temperature calculations were made for this balloon; one method assumes a homogeneous exterior surface with optical properties that are based on an area weighted average of white paint and vapor-deposited aluminum (see previous section on "Apparatus") and the other method assumes a vapor-deposited aluminum patch on the polka-dot balloon. The temperatures of the aluminized Mylar patch were determined by modifying equation (2) as follows:

$$T_{patch} = \left[\frac{1}{\sigma(\epsilon_i + \epsilon_{o,patch})}(\alpha_{s,patch}E_s \cos\theta + \epsilon_i E_i)\right]^{1/4} \tag{3}$$

where E_i is determined from equation (A4) by using average optical properties.

It is believed that the differences between measured and calculated temperatures at $\theta = -90^o$ for the Echo II and the polka-dot models are due primarily to skin conduction. See figures 19(a) and (c). Note, however, that the solar-simulator beam was convergent and some solar radiation was received by balloon areas at $\theta = -94^o$.

Figure 19(b) shows poor agreement with calculated temperatures on the cold side of the modified Echo II model. An analysis of data obtained from the radiometer located on the outside surface of this balloon indicated that portions of the liquid nitrogen liner, near $\theta = 180^{\circ}$, had become too warm. This extra heat caused the cold-side skin temperatures to be warm by the amount indicated by the 50° to 60° K differences between measured and calculated temperatures. The unwanted heat from the nitrogen liner should indirectly increase temperatures on the sun side by increasing the internal energy E_i in equation (2). Since this heating was small and its effect on E_i was small as compared with the solar heat, the skin temperature at $\theta = 0$ was not significantly affected.

Internal temperatures.- Calculated internal temperatures were obtained by dividing the balloon surface into 32 equal areas and summing the reflected and emitted energy to a unit area on the balloon diameter, that is,

$$T_e = \left[\frac{\sum_{n=0}^{32} \left(\epsilon_i \sigma T_{\Delta A,n}{}^4 + \rho E_i \right) F_{\Delta A,n}}{\sigma} \right]^{1/4} \tag{4}$$

where $T_{\Delta A}$ is given by equation (2) and E_i by equation (A2). Diffuse surfaces were assumed. The view factors used are discussed in appendix B.

Figures 20, 21, and 22 compare measured and calculated internal temperatures for the three balloon models. Figures 20 and 22 show a reasonable correlation between measured and calculated temperature levels for the Echo II and polka-dot balloons. The higher than predicted temperatures for the modified Echo II model reflect the effects of the high measured α_s/ϵ_o ratio of this balloon when the viewport was closed.

A comparison of measured and calculated temperature trends is significant in determining the validity of the diffuse assumptions used in the calculations. Figure 21 shows that the use of diffuse assumptions in the calculations predicted the uniform temperature trends measured for the modified Echo II which had a specular and highly reflective interior. This agreement might be expected since the many multiple reflections of a specular surface would tend to promote temperature uniformity. Figure 22, however, shows relatively poor agreement between measured and calculated trends for the polka-dot model which had a specular (ref. 13) but less reflective interior. Note in figure 22 the differences between measured and predicted trends near 75 percent of the balloon diameter. In all cases the temperatures were equal to or more uniform than those predicted by using diffuse assumptions in the calculations.

CONCLUSIONS

The following conclusions are made for an experimental investigation of the effectiveness of three balloon-type thermal control enclosure models in providing a uniform thermal environment for a slender, nonconducting payload:

1. The balloon enclosure with the interior surface having the highest emittance had the most uniform skin temperature.

2. The enclosure with the interior having the highest reflectance provided the most uniform thermal environment for the simulated payload. However, large skin temperature variations occurred in this model.

3. Tests of an enclosure employing an exterior surface with composite optical properties, $\frac{\alpha_S}{\epsilon_O} \approx 1.0$, and a moderately reflective interior minimized skin enclosure temperature variations and provided a relatively uniform and near-room-temperature environment for the simulated payload.

4. Test results indicate that payload internal temperature uniformities within 6° K are feasible for surfaces near the center of the enclosure. For the best temperature uniformity the payload should be centrally located.

5. Diffuse-type calculations predicted payload temperature trends when the interior surface of the enclosure was diffuse and when the interior was specular and highly reflective. Considerable differences between measured and predicted trends resulted when the interior surface was specular and only moderately reflective.

Langley Research Center,
    National Aeronautics and Space Administration,
        Hampton, Va., April 20, 1971.

APPENDIX A

HEAT RADIATED THROUGH AN OPENING IN A BALLOON

For some applications a viewport or balloon opening may be required to allow the enclosed payload to view space or to dissipate payload heat or both. In the present discussion only solar heating is considered and the enclosed payload is assumed small as compared with the balloon; that is, radiation blockage by the payload is neglected.

Reference 2, for example, shows that the radiant heat emanating from an element of inside balloon surface is equally dispersed to all other wall elements. The total radiant energy incident to an inside wall element E_i (ref. 2) may be written as

$$E_i = \frac{1}{4\pi r^2} \int_0^{2\pi} \int_0^{\pi/2} \left\{ \epsilon_i \sigma T_{\theta\phi}{}^4 + (1 - \epsilon_i)\frac{Q}{4\pi r^2} + \frac{(1 - \epsilon_i)}{\epsilon_i}\left[\sigma T_{\theta\phi}{}^4(\epsilon_i + \epsilon_o) - \alpha_i \frac{Q}{4\pi r^2} \right. \right.$$

$$\left. - \alpha_s E_s \cos\theta \right\} r^2 \sin\theta \, d\theta \, d\phi + \frac{1}{4\pi r^2} \int_0^{2\pi} \int_{\pi/2}^{\pi} \left\{ \epsilon_i \sigma T_{\theta\phi}{}^4 + (1 - \epsilon_i)\frac{Q}{4\pi r^2} \right.$$

$$\left. + \frac{(1 - \epsilon_i)}{\epsilon_i}\left[\sigma T_{\theta\phi}{}^4(\epsilon_i + \epsilon_o) - \alpha_i \frac{Q}{4\pi r^2} \right] \right\} r^2 \sin\theta \, d\theta \, d\phi \tag{A1}$$

Figure 23 defines θ and ϕ which locate the wall element with respect to the solar vector. The second integral represents the contribution of elements that do not receive solar heat. Because the skin temperature in this hemisphere is constant, all elements contribute equally to E_i. For a viewport located in this hemisphere the energy contribution to E_i would be reduced in proportion to the spherical area removed. Multiplying the second integral term in equation (A1) by the fraction of the remaining area, $1 - \frac{A_{sc}}{2\pi r^2}$, and simplifying gives

$$E_i = \frac{1}{4\pi}\left(\frac{1}{\epsilon_o} + \frac{1}{\epsilon_i} - 1\right)\sigma\epsilon_o\left[\int_0^{2\pi} \int_0^{\pi/2} T_{\theta\phi}{}^4 \sin\theta \, d\theta \, d\phi + \left(1 - \frac{A_{sc}}{2\pi r^2}\right) \right.$$

$$\left. + \left(1 - \frac{A_{sc}}{2\pi r^2}\right) \int_0^{2\pi} \int_{\pi/2}^{\pi} T_{\theta\phi}{}^4 \sin\theta \, d\theta \, d\phi \right] - \frac{1}{4}\left(\frac{1 - \epsilon_i}{\epsilon_i}\right)\alpha_s E_s \tag{A2}$$

13

The integral terms in equation (A2) can be solved for directly from an energy balance of the entire balloon:

$$\sum E_{balloon} = 0$$

$$= -\sigma\epsilon_o\left[\int_0^{2\pi}\int_0^{\pi/2} T_{\theta\phi}{}^4\sin\theta\ d\theta\ d\phi + \left(1 - \frac{A_{sc}}{2\pi r^2}\right)\int_0^{2\pi}\int_{\pi/2}^{\pi} T_{\theta\phi}{}^4\sin\theta\ d\theta\ d\phi\right]$$

$$+ \pi\alpha_s E_s + \left(1 - \frac{A_{sc}}{4\pi r^2}\right)\frac{Q}{r^2} - A_{sc}\frac{E_i}{r^2} \qquad (A3)$$

Combining equations (A2) and (A3) yields the internal energy term E_i as

$$E_i = \frac{1}{1 + \dfrac{A_{sc}}{4\pi r^2}\left(\dfrac{1}{\epsilon_o} + \dfrac{1}{\epsilon_i} - 1\right)}\left[\frac{\alpha_s E_s}{4\epsilon_o} + \frac{Q}{4\pi r^2}\left(1 - \frac{A_{sc}}{4\pi r^2}\right)\left(\frac{1}{\epsilon_o} + \frac{1}{\epsilon_i} - 1\right)\right] \qquad (A4)$$

The total energy leaving through the spherical cap removed from the balloon is the sum of direct source heat and the internal energy, that is,

$$Q_{vp} = A_{sc}\left(E_i + \frac{Q}{4\pi r^2}\right) \qquad (A5)$$

where

$$A_{sc} = 2\pi r\left(r - \sqrt{r^2 - r_{vp}}\right)$$

APPENDIX B

VIEW FACTOR BETWEEN A BALLOON WALL AREA AND A UNIT AREA

LOCATED ON A BALLOON DIAMETER

The view factor between a unit area located on a balloon diameter and a finite balloon area may be written as

$$F_{\Delta A} = \frac{\cos \chi_1 \cos \chi_2 \Delta A}{\pi d^2} \tag{B1}$$

where χ_1 and χ_2 are angles between the normals to the areas and a directed line d connecting the areas. Using the notation presented in figure 24 gives

$$\cos \chi_1 = \frac{\cos \beta}{d}$$

$$\cos \chi_2 = \frac{1 - a \cos \delta \sin \beta}{d}$$

and

$$d = \frac{1 - a \cos \delta \sin \beta + a^2}{d}$$

substituting these equations into equation (B1) yields

$$F_{\Delta A} = \frac{\cos \beta (1 - a \cos \delta \sin \beta)}{\pi (1 - 2a \cos \delta \sin \beta + a^2)^2} \tag{B2}$$

The spherical surface was divided into 32 equal areas whose centers are described by the apex and centerfaces of an inscribed icosahedron. (See fig. 25). Because of symmetry only 11 view factors required determination for each value of ϕ. These calculations were carried out on a desk-type calculator. Equation (B2), however, will result in considerable error when the diametral area is close to the balloon wall, that is, when a approaches r. The view factor for area 1, figure 25, was obtained more accurately from data presented in reference 14.

REFERENCES

1. Spitzer, Lyman, Jr.: The Beginnings and Future of Space Astronomy. Amer. Sci., vol. 50, Sept. 1962, pp. 473-484.

2. Sweet, George E.: An Experimental and Analytical Investigation of Balloon-Type Enclosures for Thermal Control of Satellites. NASA TN D-5230, 1969.

3. Spacecraft Organization, Lockheed-California Co.: Expandable Structures Design Handbook. ASD-TDR-63-4275, Pt. II, U.S. Air Force, June 1965.

4. Anon.: Transactions of the Third Aerospace Expandable and Modular Structures Conference. AFAPL TR 68-17, U.S. Air Force, 1967.

5. Coffee, Claude W., Jr.; Bressette, Walter E.; and Keating, Gerald M.: Design of the NASA Lightweight Inflatable Satellites for the Determination of Atmospheric Density at Extreme Altitudes. NASA TN D-1243, 1962.

6. Clark, Lenwood G.: Temperature Balance of Manned Space Stations. A Report on the Research and Technological Problems of Manned Rotating Spacecraft, NASA TN D-1504, 1962, pp. 21-31.

7. Clemmons, Dewey L., Jr.; and Camp, John D.: Amorphous Phosphate Coatings for Thermal Control of Echo II. Electrochem. Technol., vol. 2, no. 7-8, July-Aug. 1964, pp. 221-232.

8. Woerner, Charles V.: Properties of Two White Paints for Application to Inflatable Spacecraft: Titanium-Dioxide-Pigmented Epoxy and Zinc-Oxide-Pigmented Methyl Silicone Elastomer. NASA TN D-2834, 1965.

9. Sweet, George E.; and Miller, Howard B.: A Radiometer for Use in Thermal Studies of Spacecraft. NASA TN D-4925, 1968.

10. Goethert, B. H.: Space Simulation Chambers and Techniques. AGARDograph 93, Dec. 1964.

11. Nichols, Lester D.: Surface-Temperature Distribution on Thin-Walled Bodies Subjected to Solar Radiation in Interplanetary Space. NASA TN D-584, 1961.

12. Katzoff, S.: Similitude in Thermal Models of Spacecraft. NASA TN D-1631, 1963.

13. Romick, D. C.; Emmons, R. H.; Preski, R. J.; and Kalasky, E. D.: The Modification and Use of a Ground-Based Photometer for Evaluation of Satellite Materials. GER-13830 (Contract NAS 1-6436), Goodyear Aerospace Corp., June 7, 1968. (Available as NASA CR-66772.)

14. Kreith, Frank: Radiation Heat Transfer for Spacecraft and Solar Power Plant Design. International Textbook Co., c.1962.
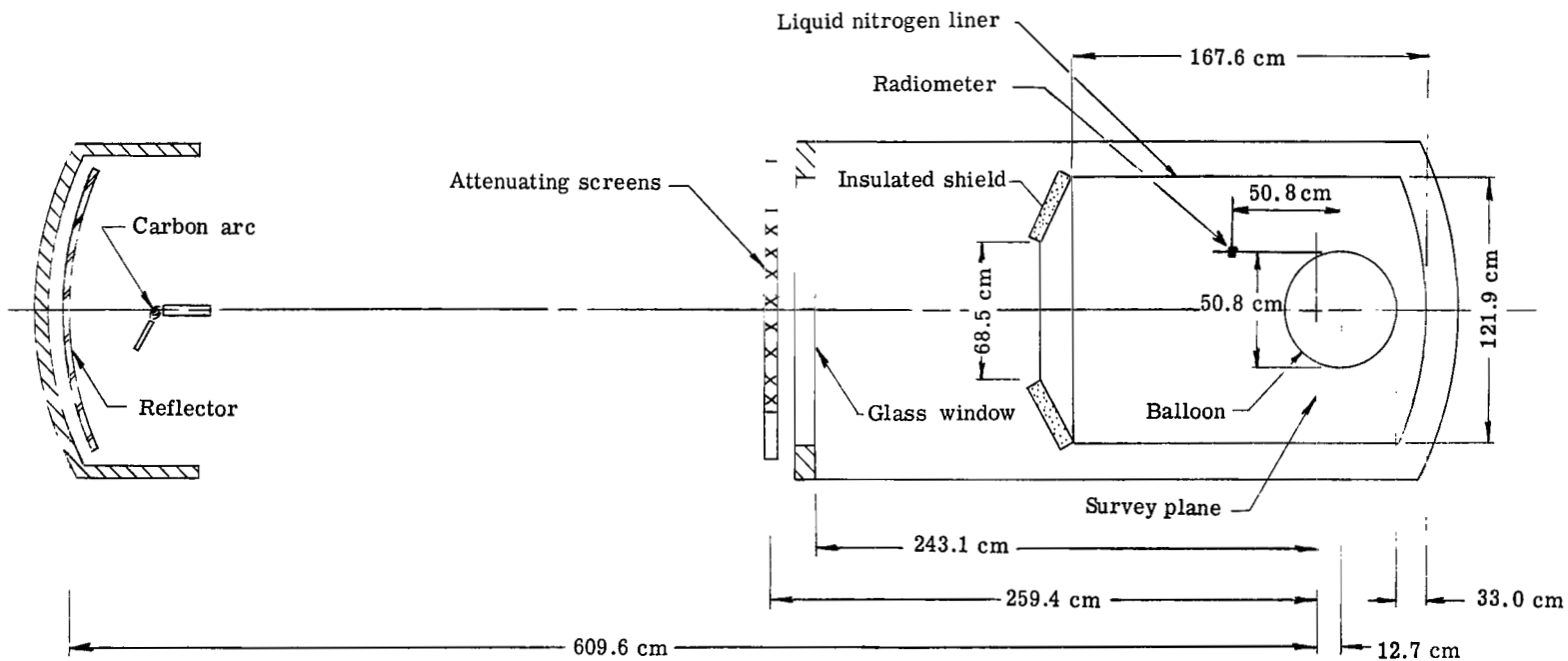
Figure 1.- General arrangement of test models and apparatus.
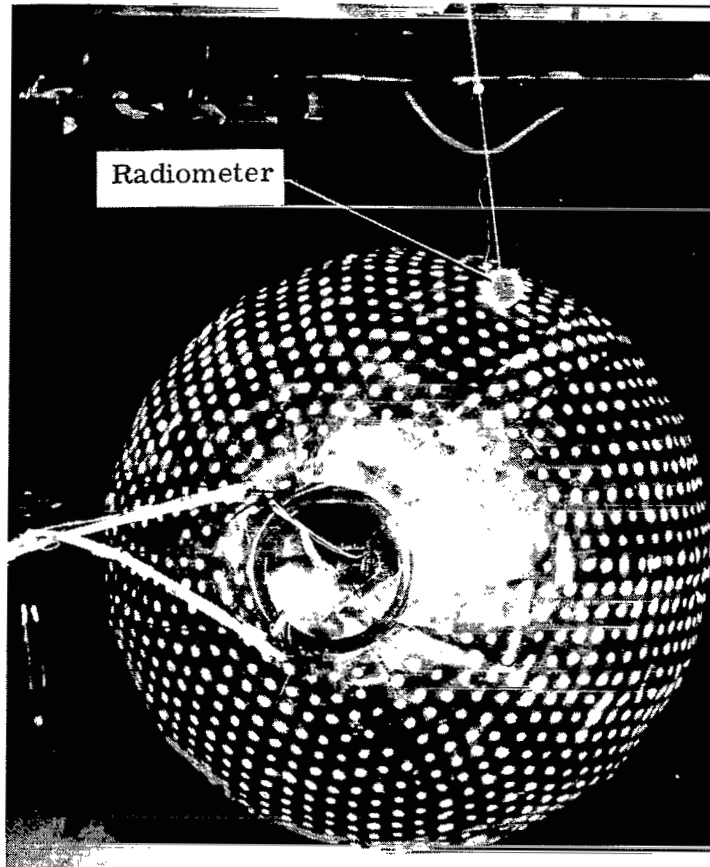
L-68-5673.1

Figure 2.- Photograph of polka-dot balloon mounted on yoke.

Radiometers

Support yoke

Fiber-glass annulus
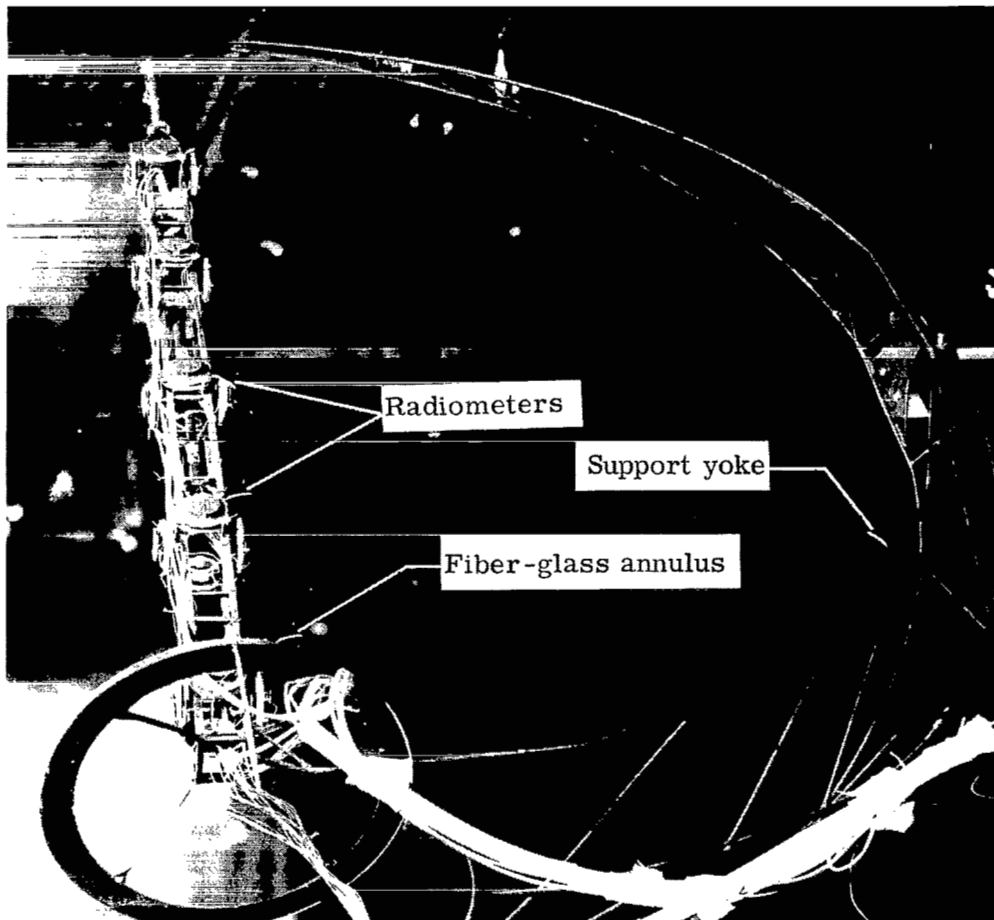
L-66-3012.2

Figure 3.- Photograph showing mounted radiometers and model support yoke.
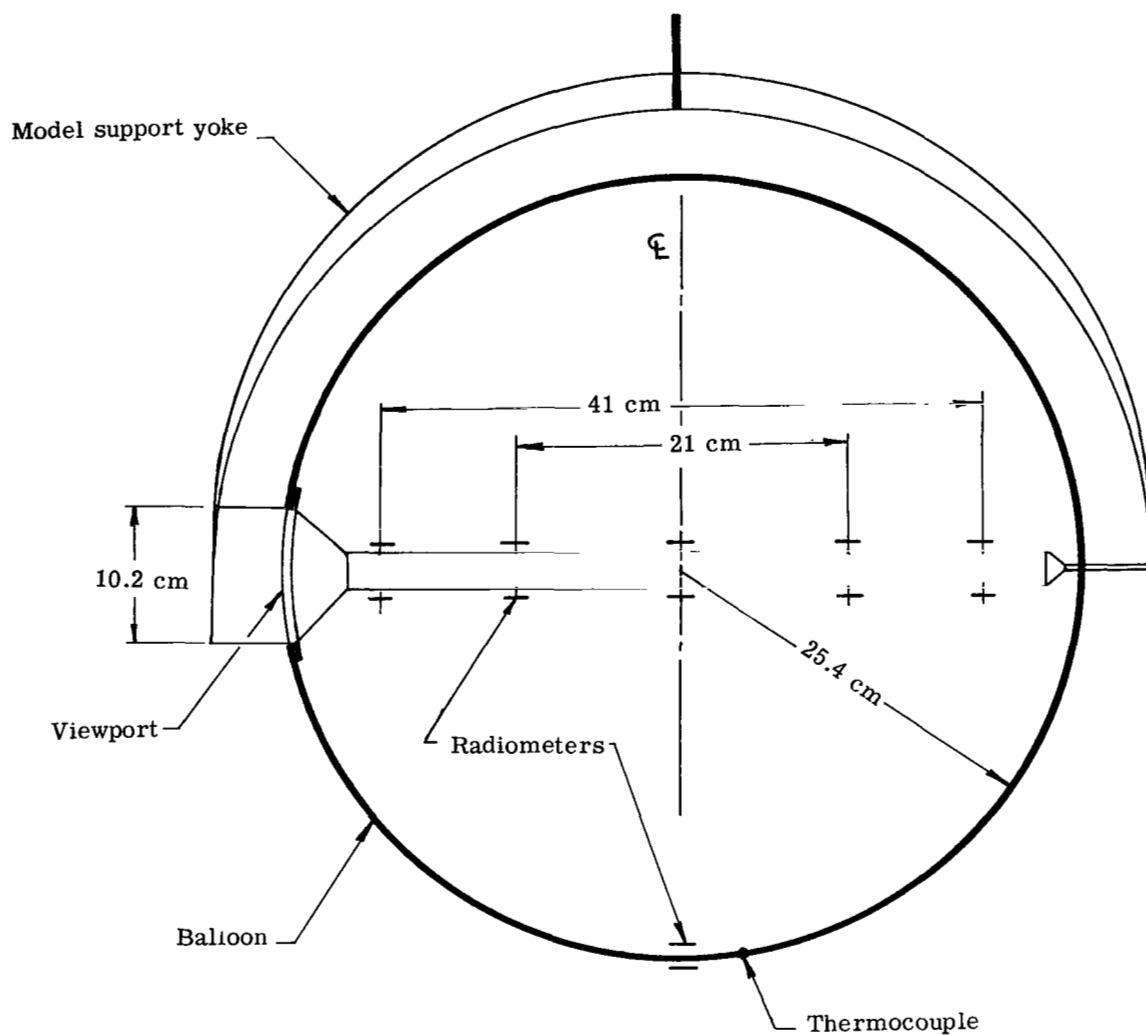
Figure 4.- Schematic diagram of model showing instrumentation locations.
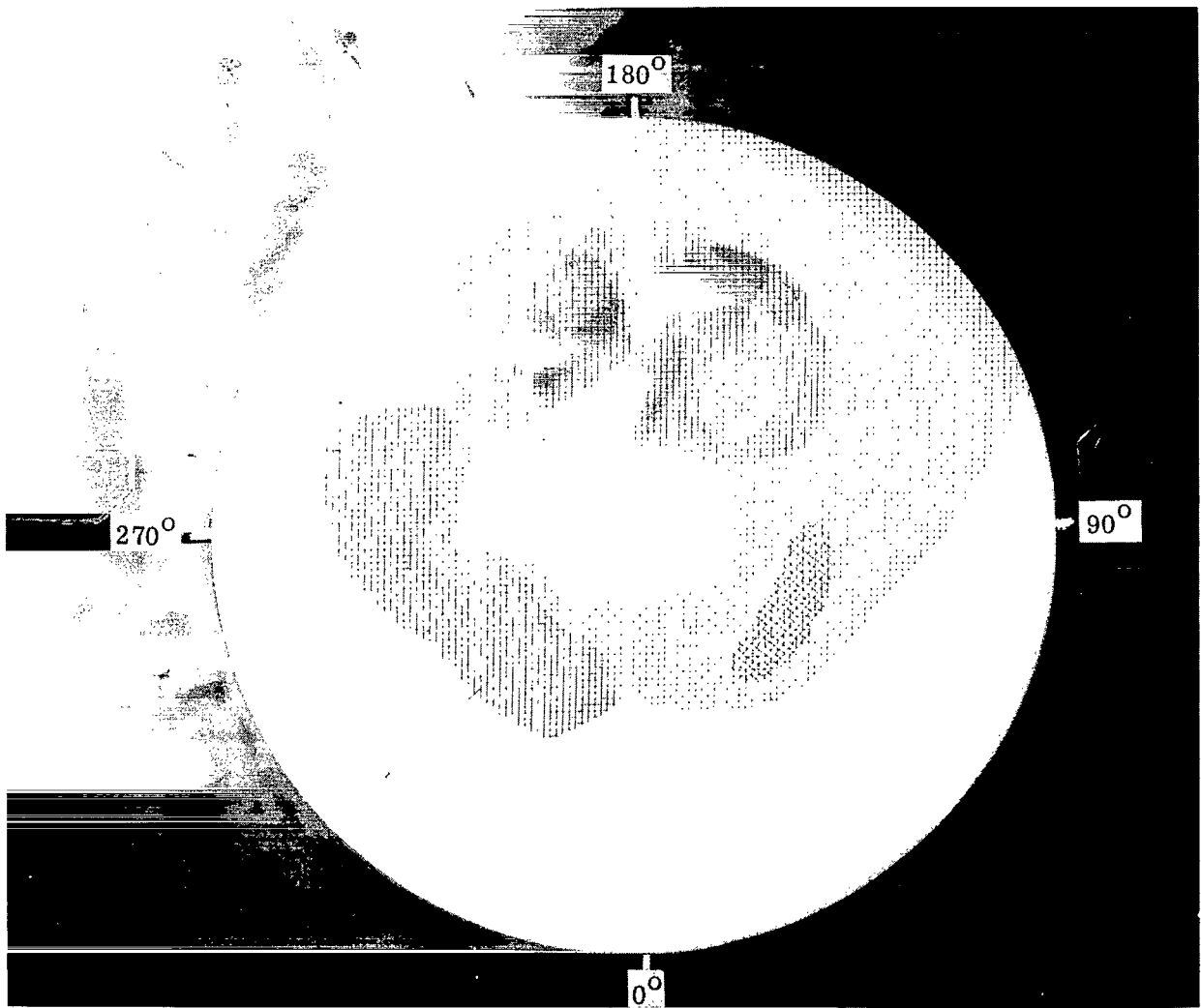
Figure 5.- Attenuating screens used for improving irradiance uniformity at survey plane.

L-65-3875.1
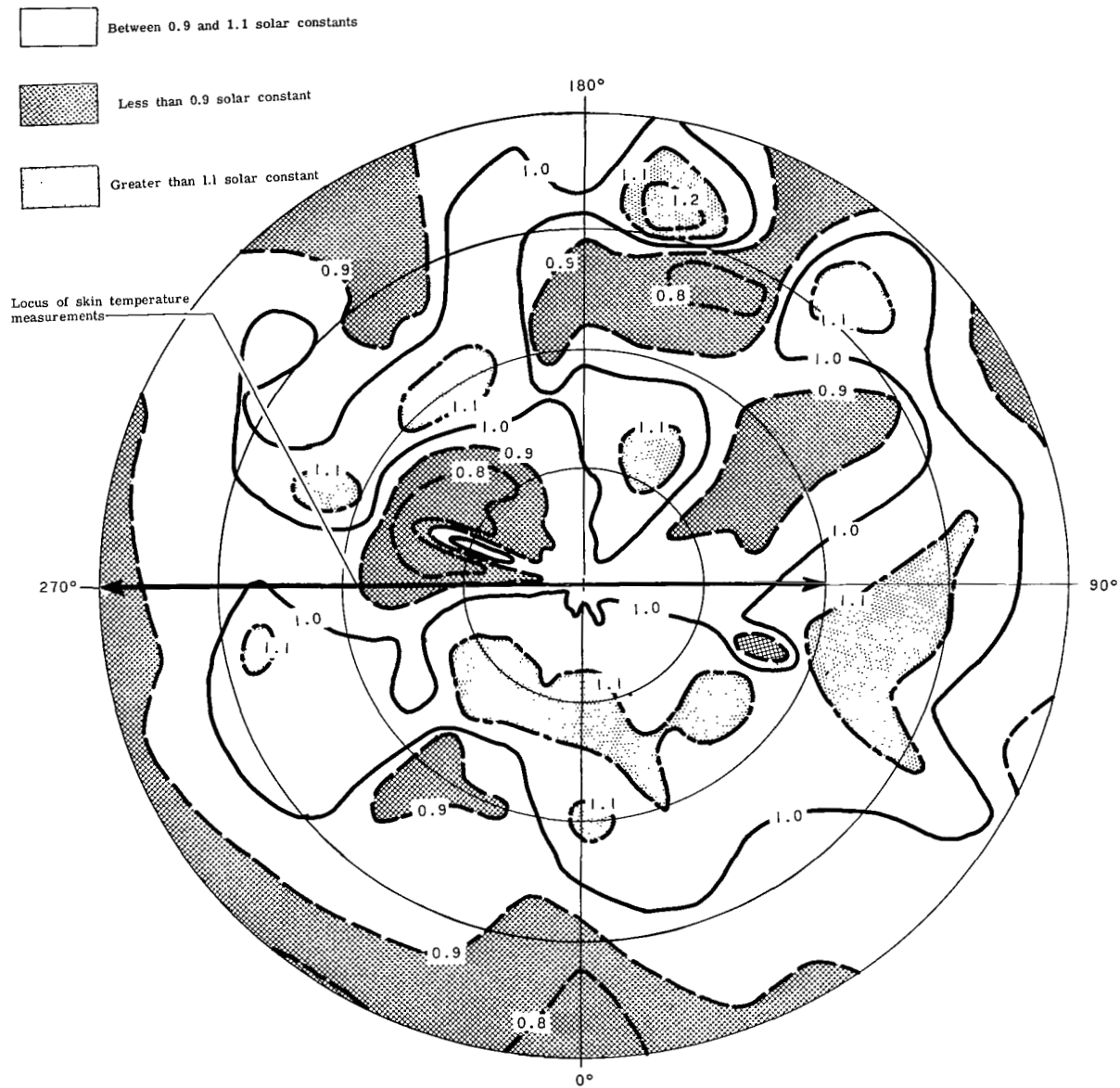
Figure 6.- Contours of constant irradiance over a 50.8-cm-diameter circle
at survey plane.
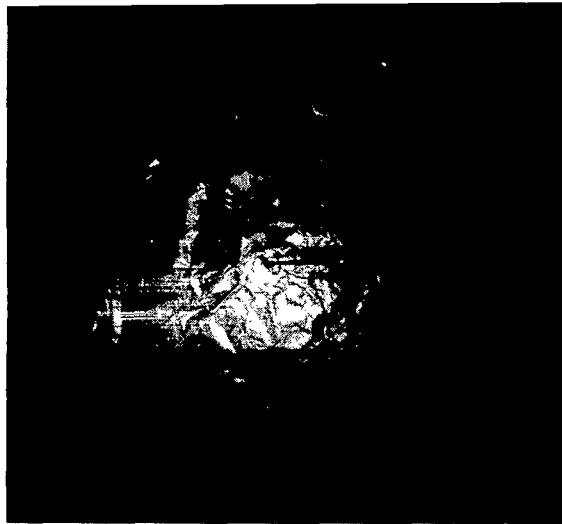
L-66-2734

Figure 7.- Distortion and wrinkling of modified Echo II
balloon due to heat shrinkage of aluminized Mylar
after temperature measurements.
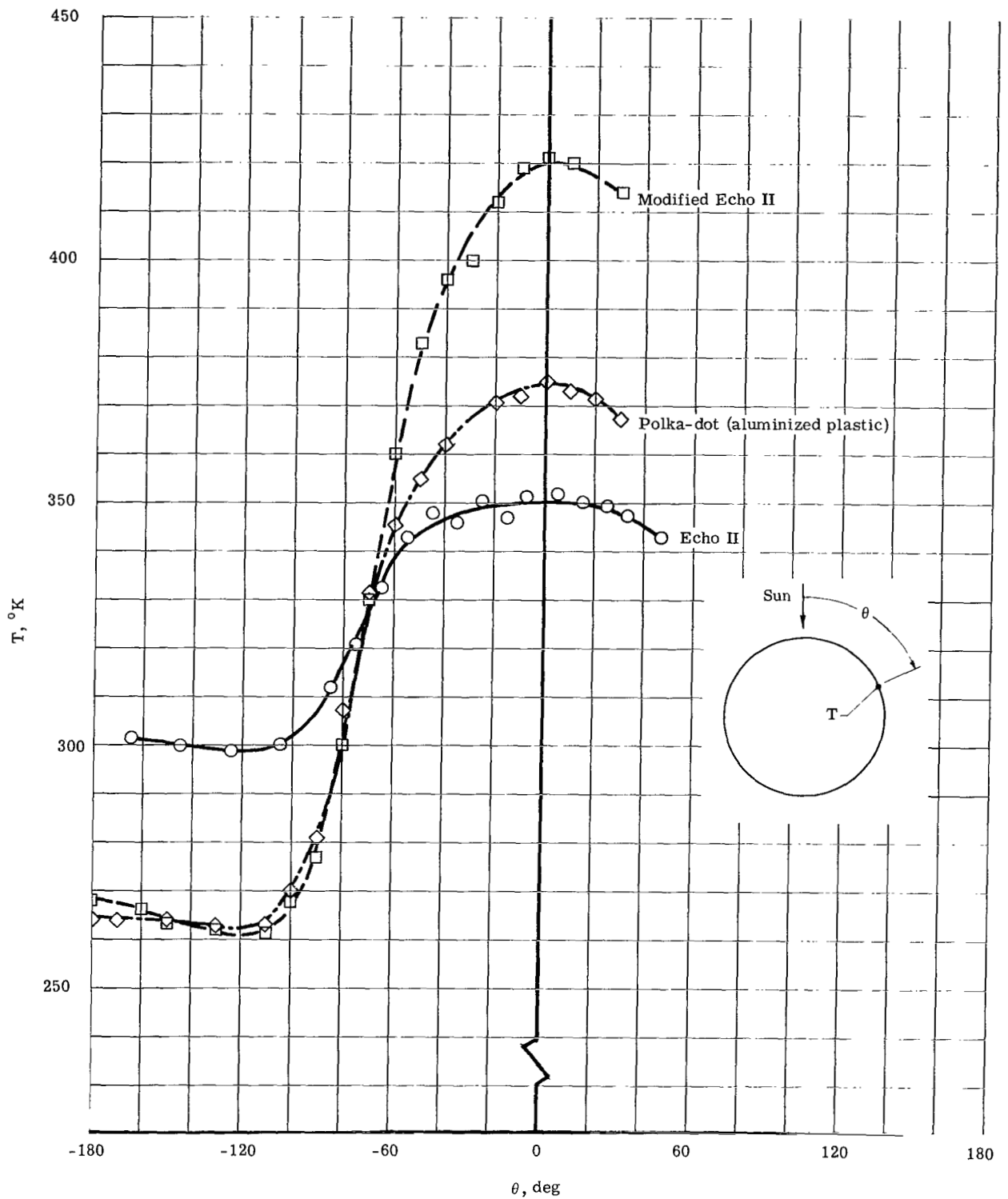
Figure 8.- Measured skin temperatures for test balloons.
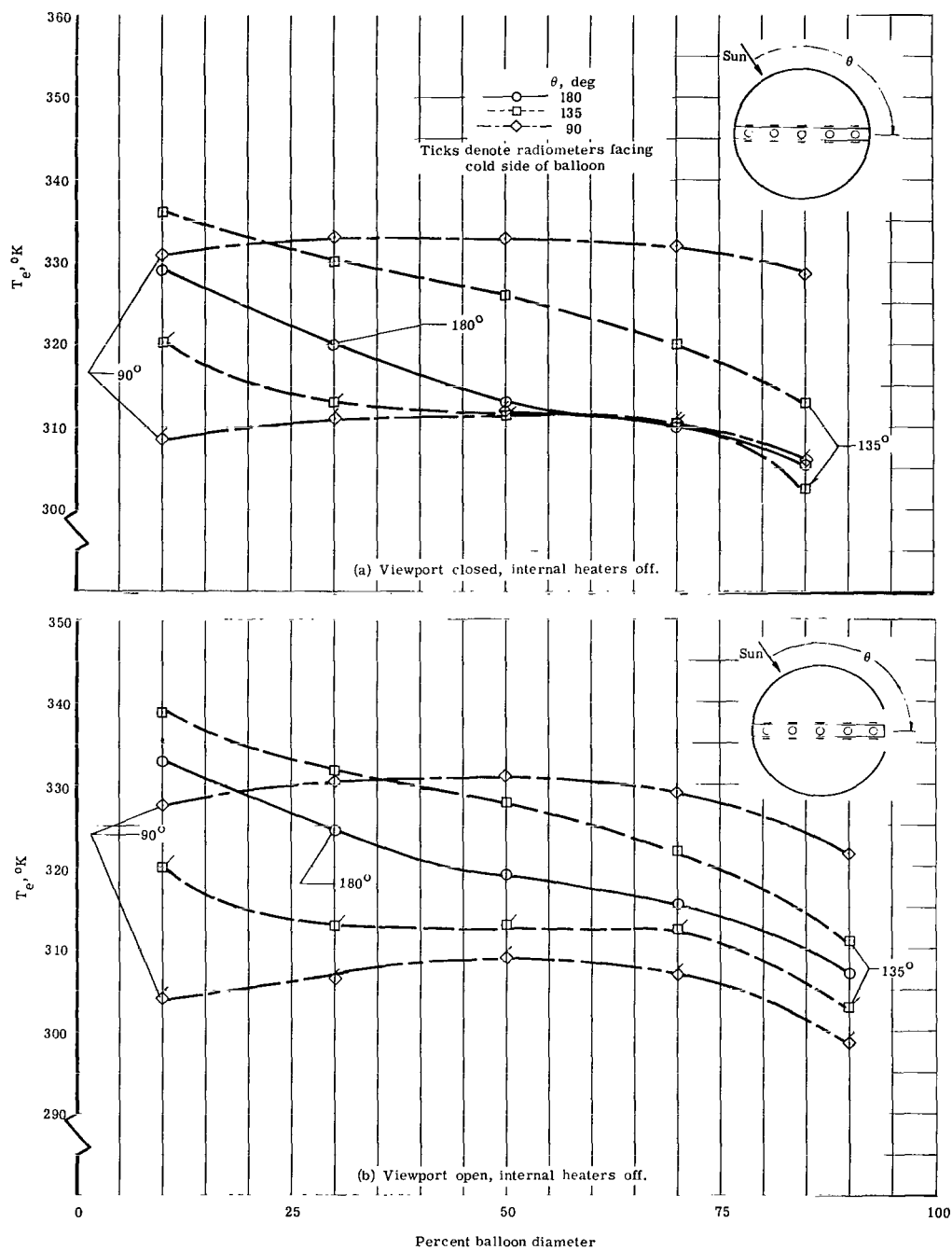
Figure 9.- Internal irradiance distributions of Echo II balloon as a function of model orientation with respect to the solar simulator. Viewport located at 100-percent diameter.

25

(c) Viewport closed, internal heaters operating, 4.64 watts.

(d) Viewport open, internal heaters operating, 4.64 watts.

Percent balloon diameter
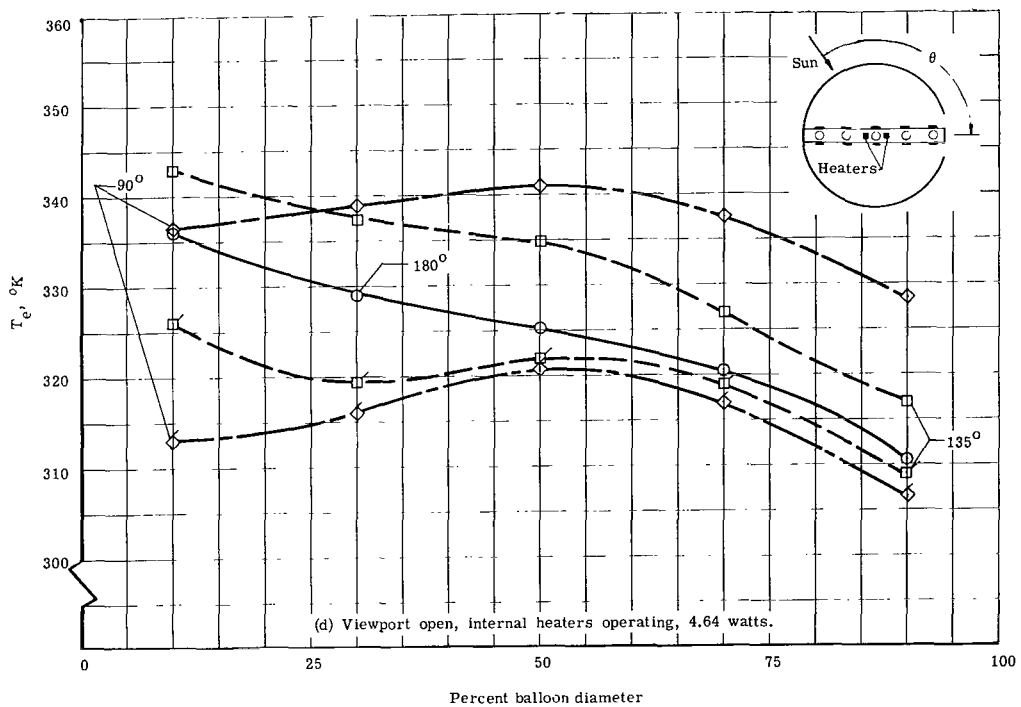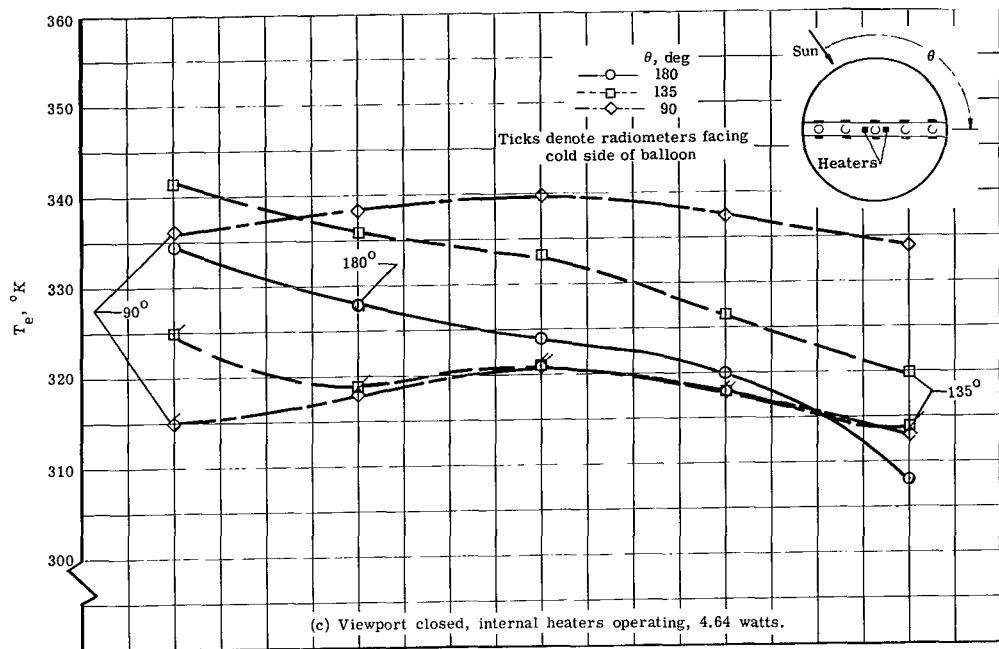
Figure 9.- Concluded.
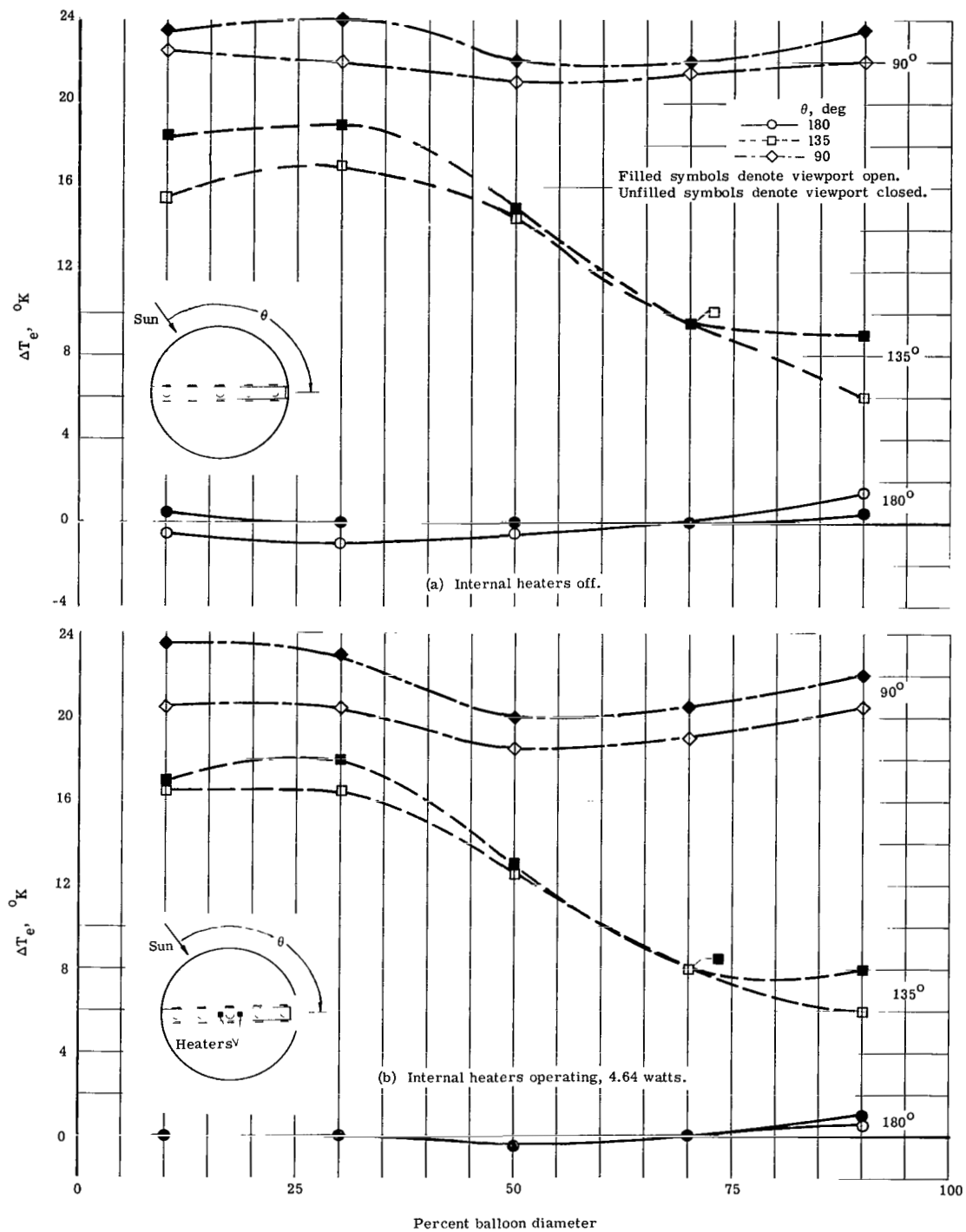
Figure 10.- Effect of viewport on temperature differences between oppositely facing radiometers for Echo II model.
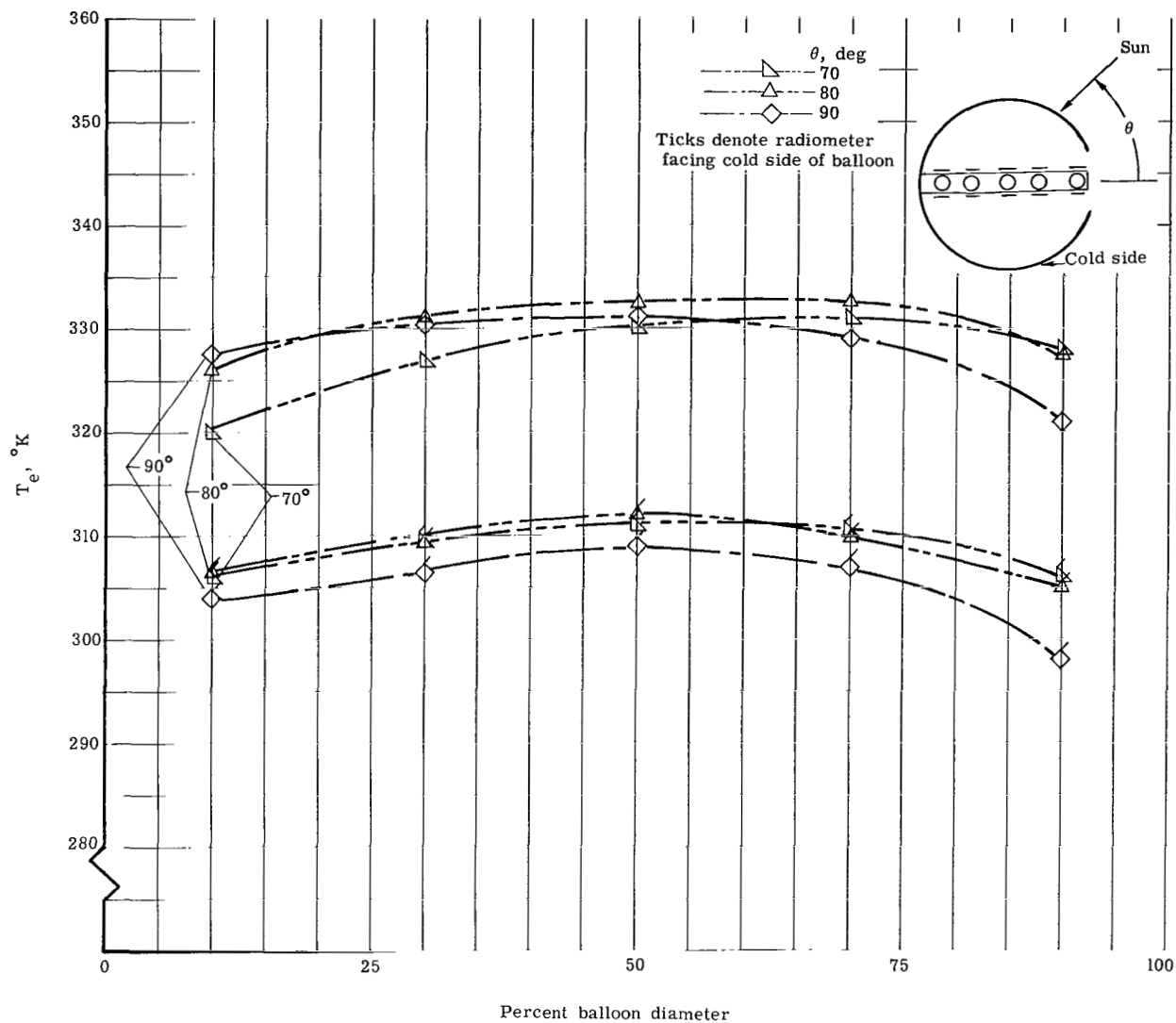
Figure 11.- Effect of simulated sunlight entering viewport of
Echo II model on internal irradiances.
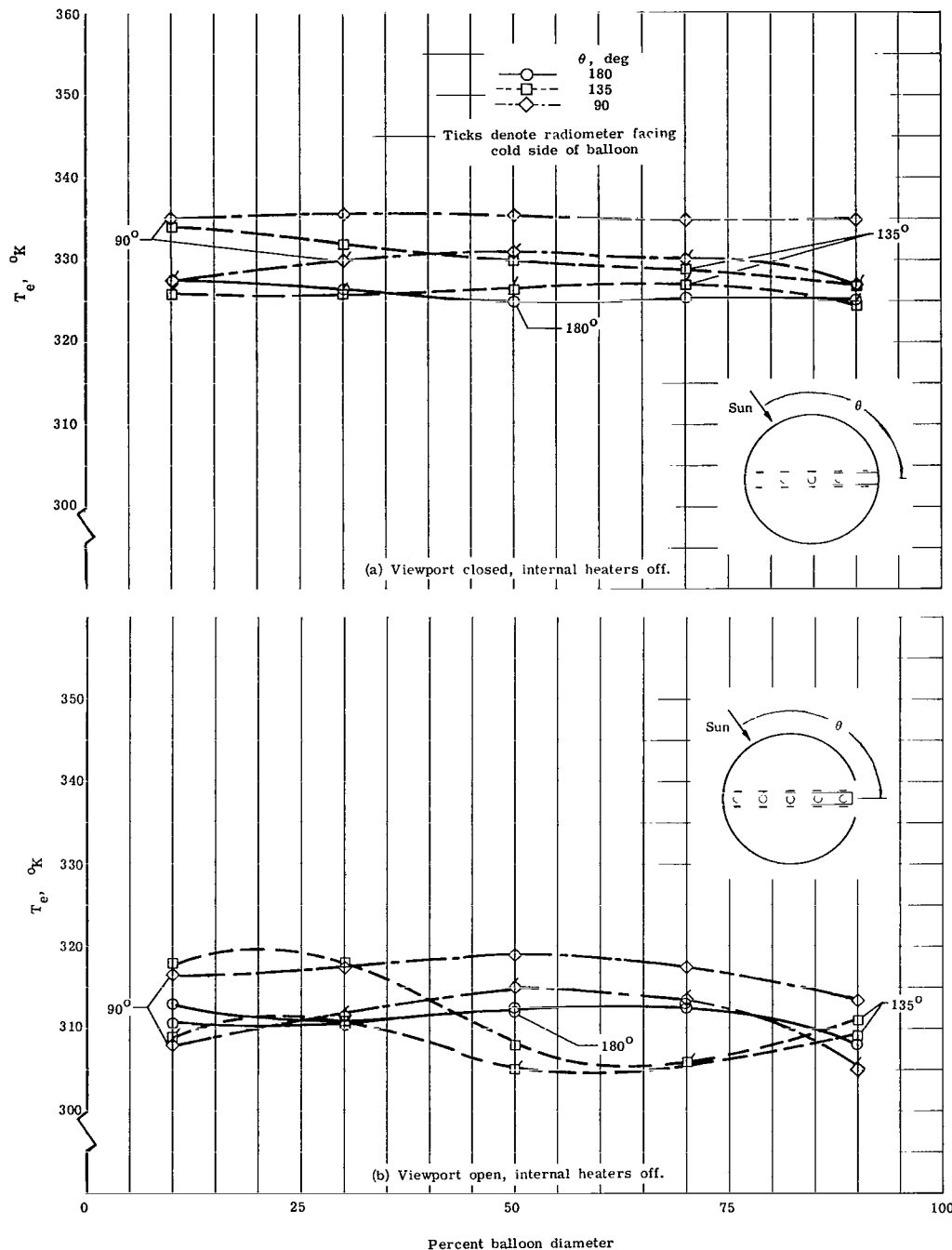
Figure 12.- Internal irradiance distributions of modified Echo II balloon as
a function of model orientation with respect to solar simulator.
Viewport located at 100-percent diameter.
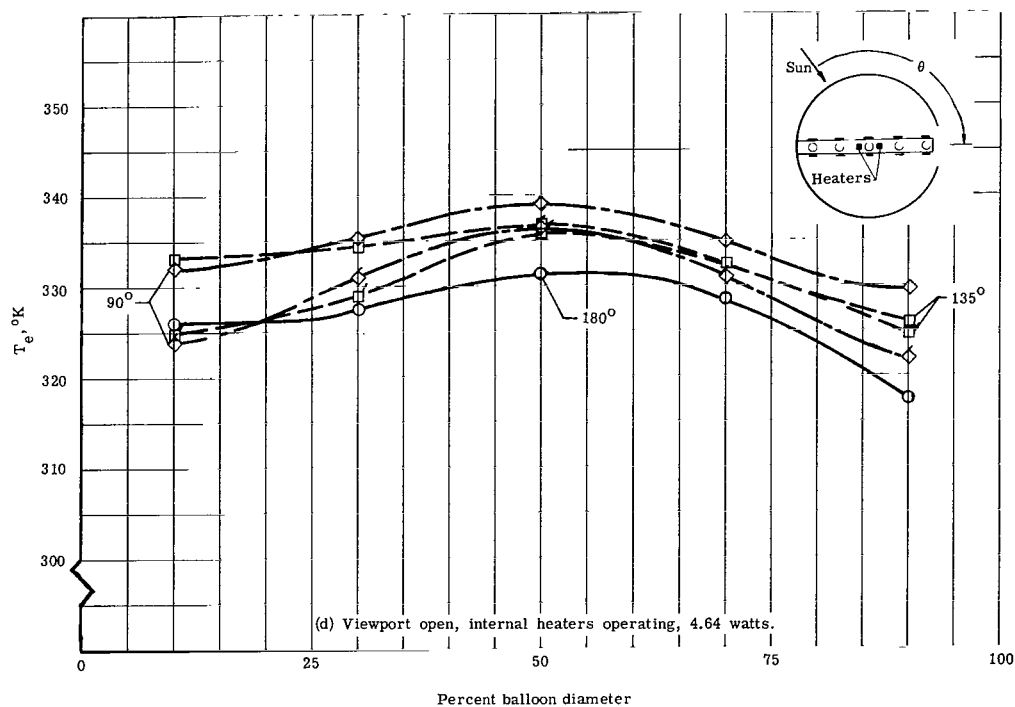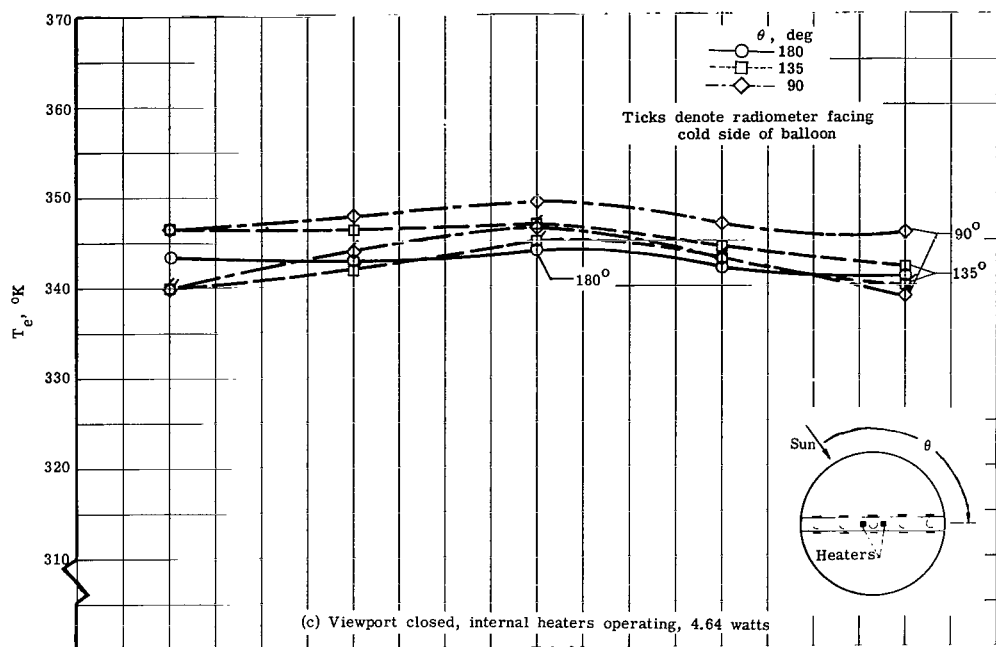
Figure 12.- Concluded.
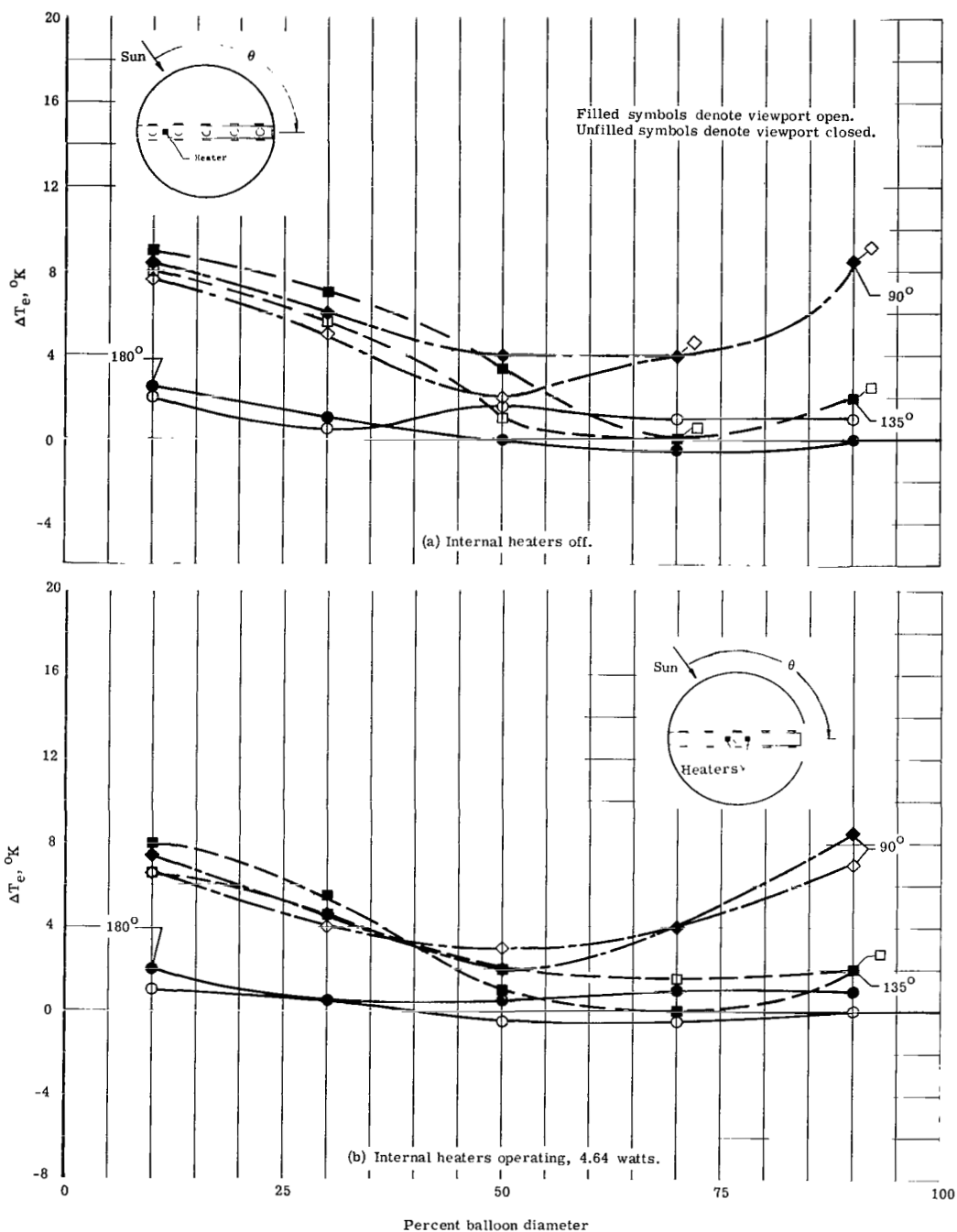
Figure 13.- Effect of viewport on temperature differences between oppositely facing radiometers for modified Echo II model.
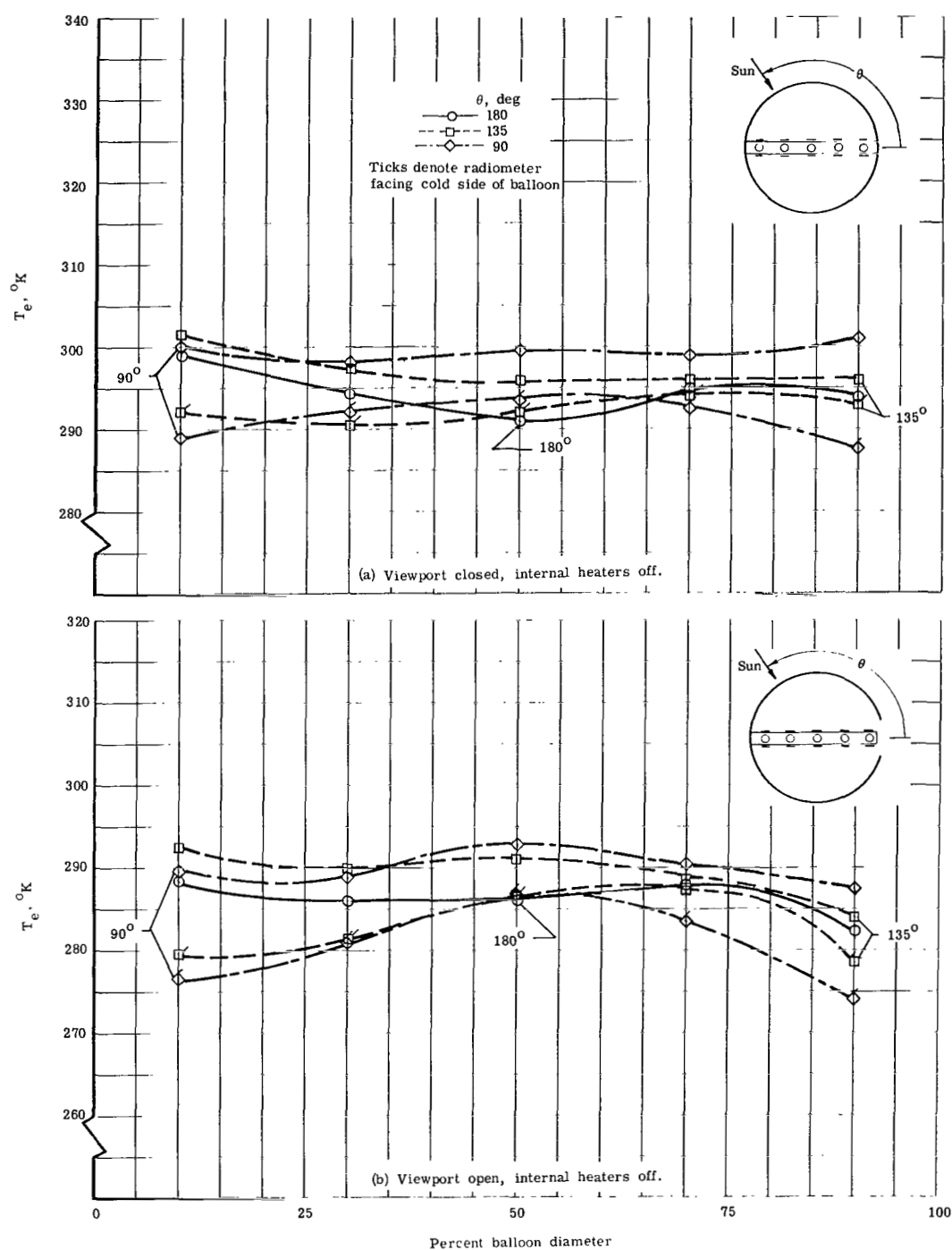
Figure 14.- Internal irradiance distributions of polka-dot balloon model as a function of model orientation with respect to solar simulator. Viewport located at 100-percent diameter.

(c) Viewport closed, internal heaters operating, 4.64 watts.

(d) Viewport open, internal heaters operating, 4.64 watts.

Percent balloon diameter
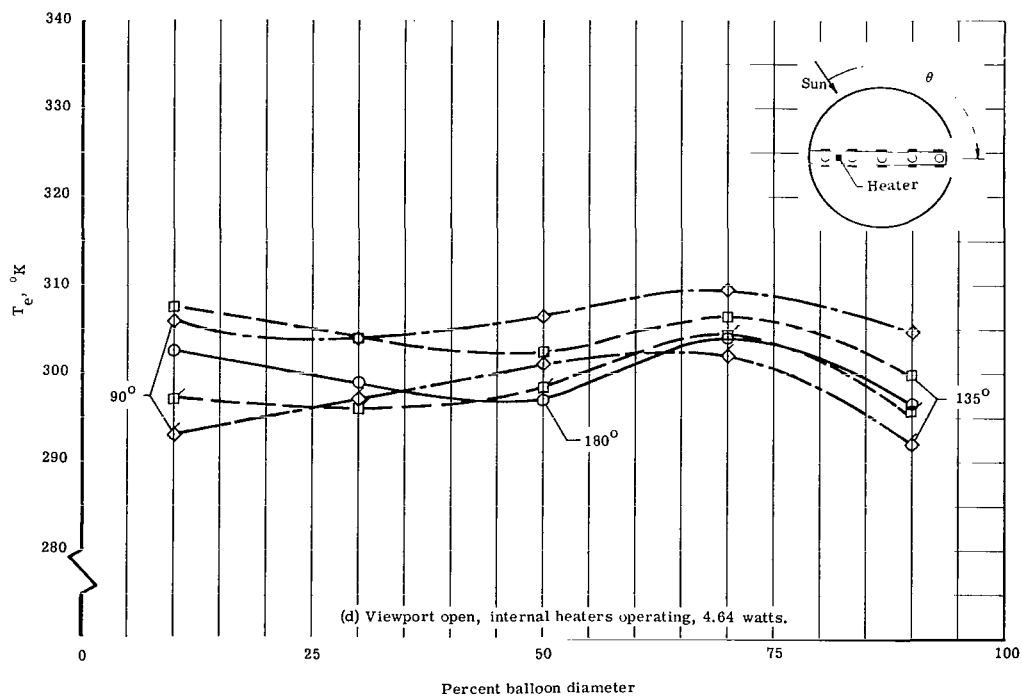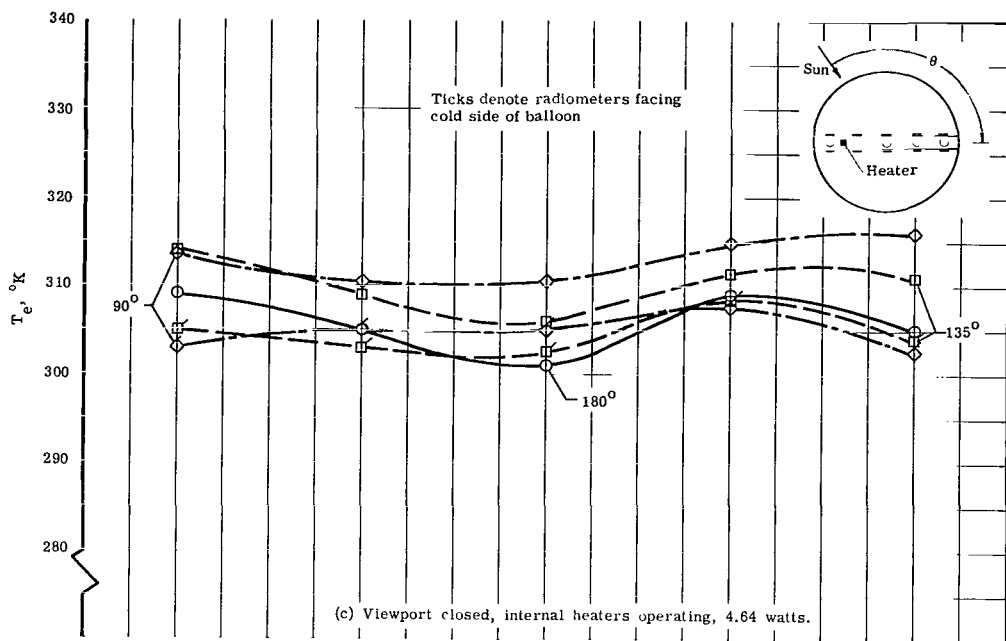
Figure 14.- Concluded.
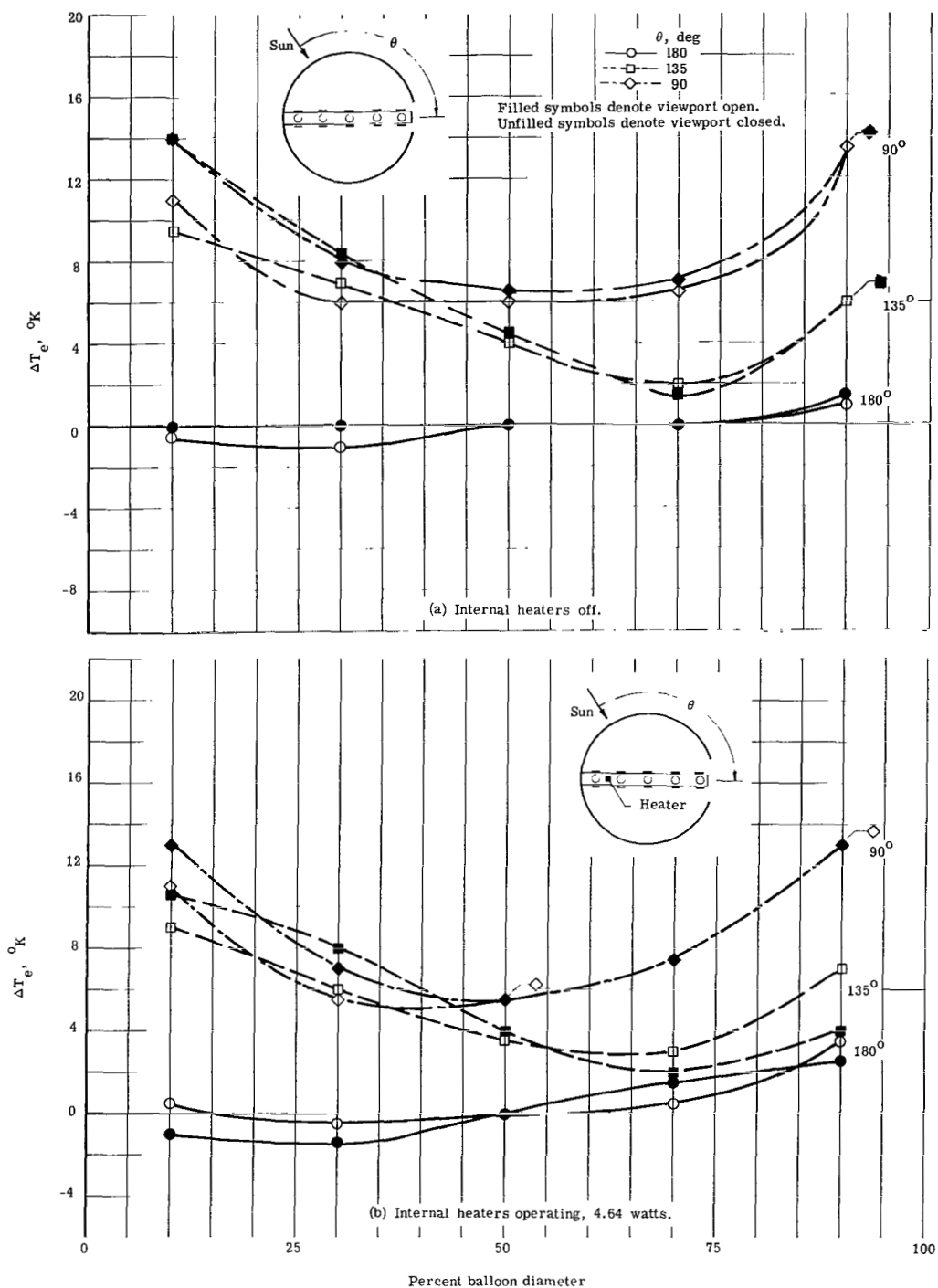
Figure 15.- Effect of viewport on temperature differences between oppositely facing radiometers for polka-dot balloon model.
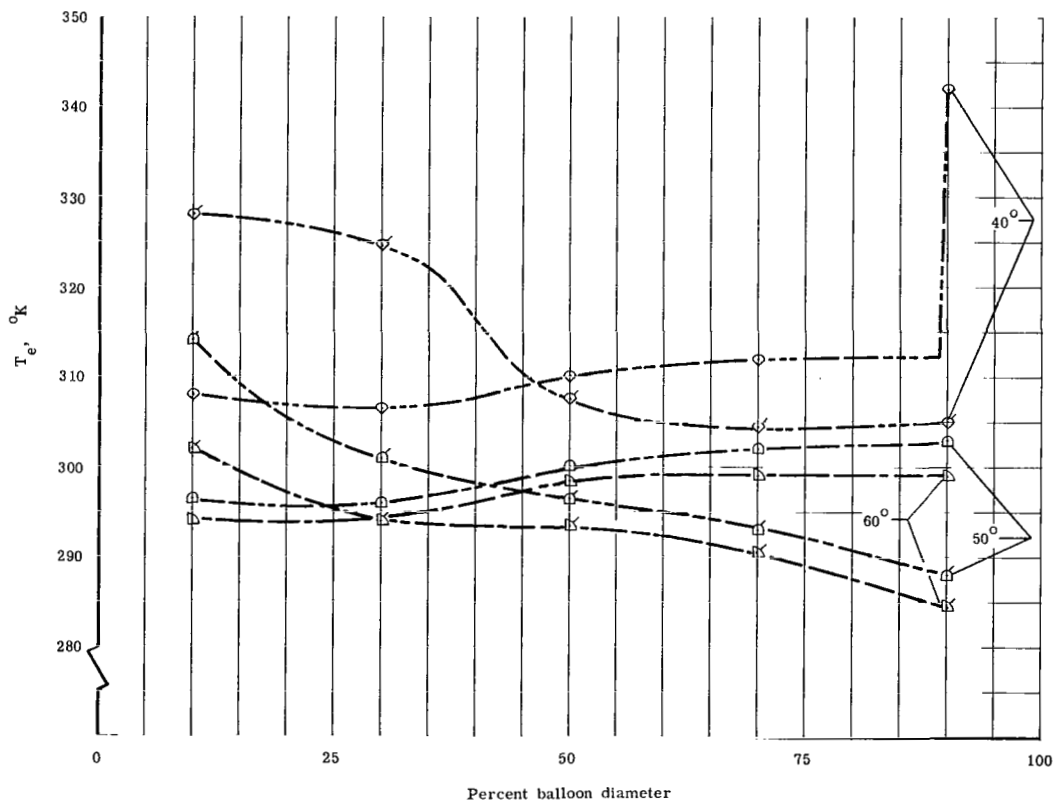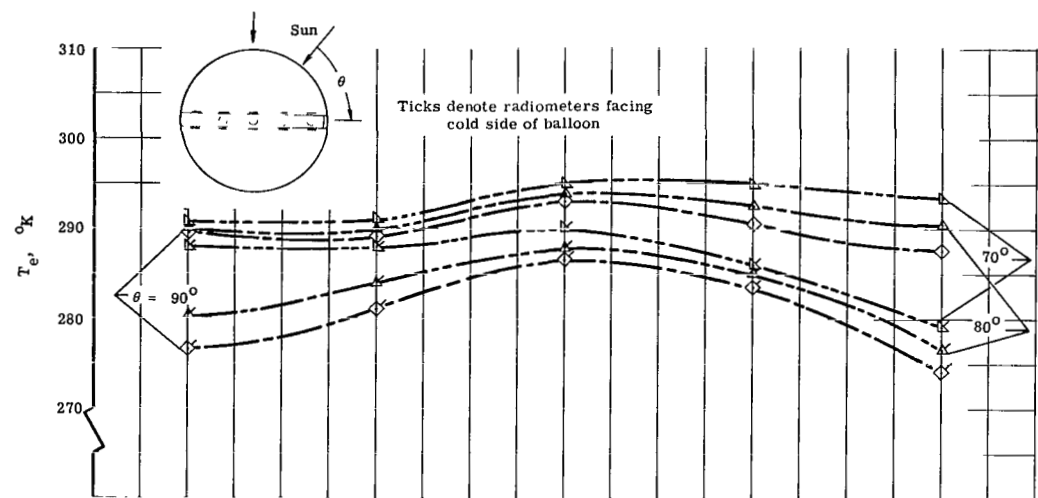
Figure 16.- Effect of simulated sunlight entering viewport of
the polka-dot model on internal irradiances.
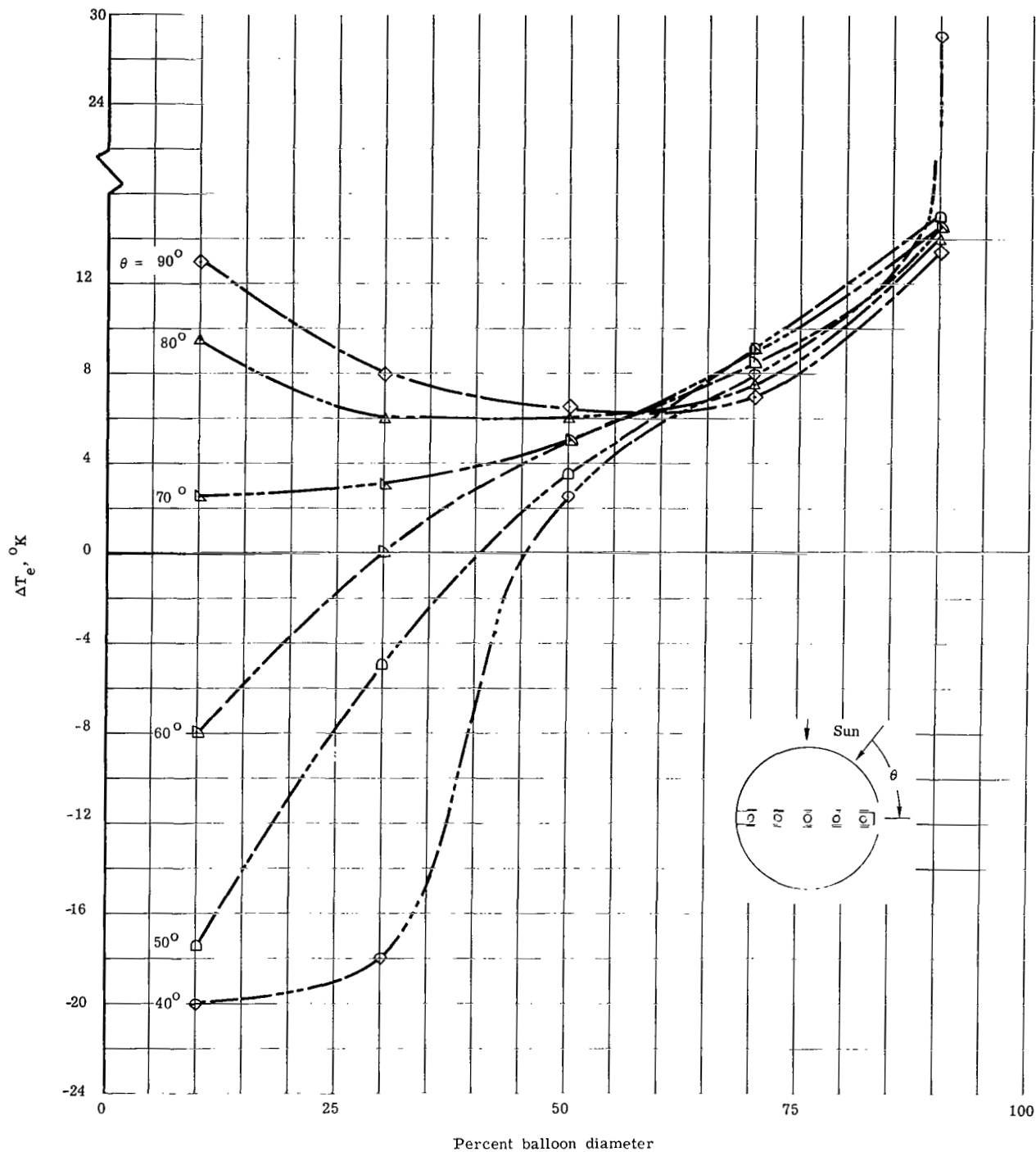
Figure 17.- Effect of simulated sunlight entering viewport of polka-dot balloon on temperature differences between oppositely facing radiometers, ΔT.
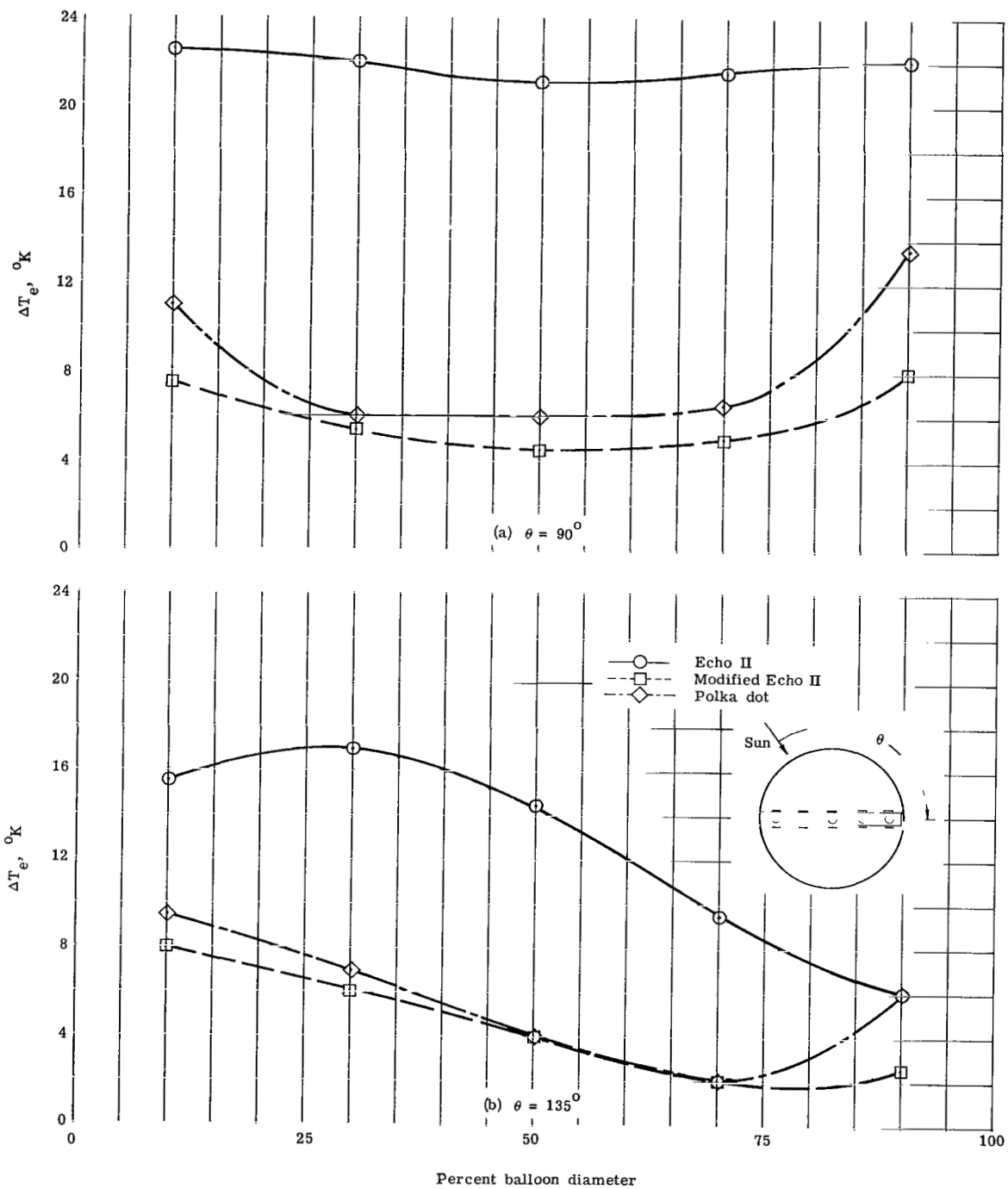
Figure 18.- Comparison of temperature uniformity for test balloons.
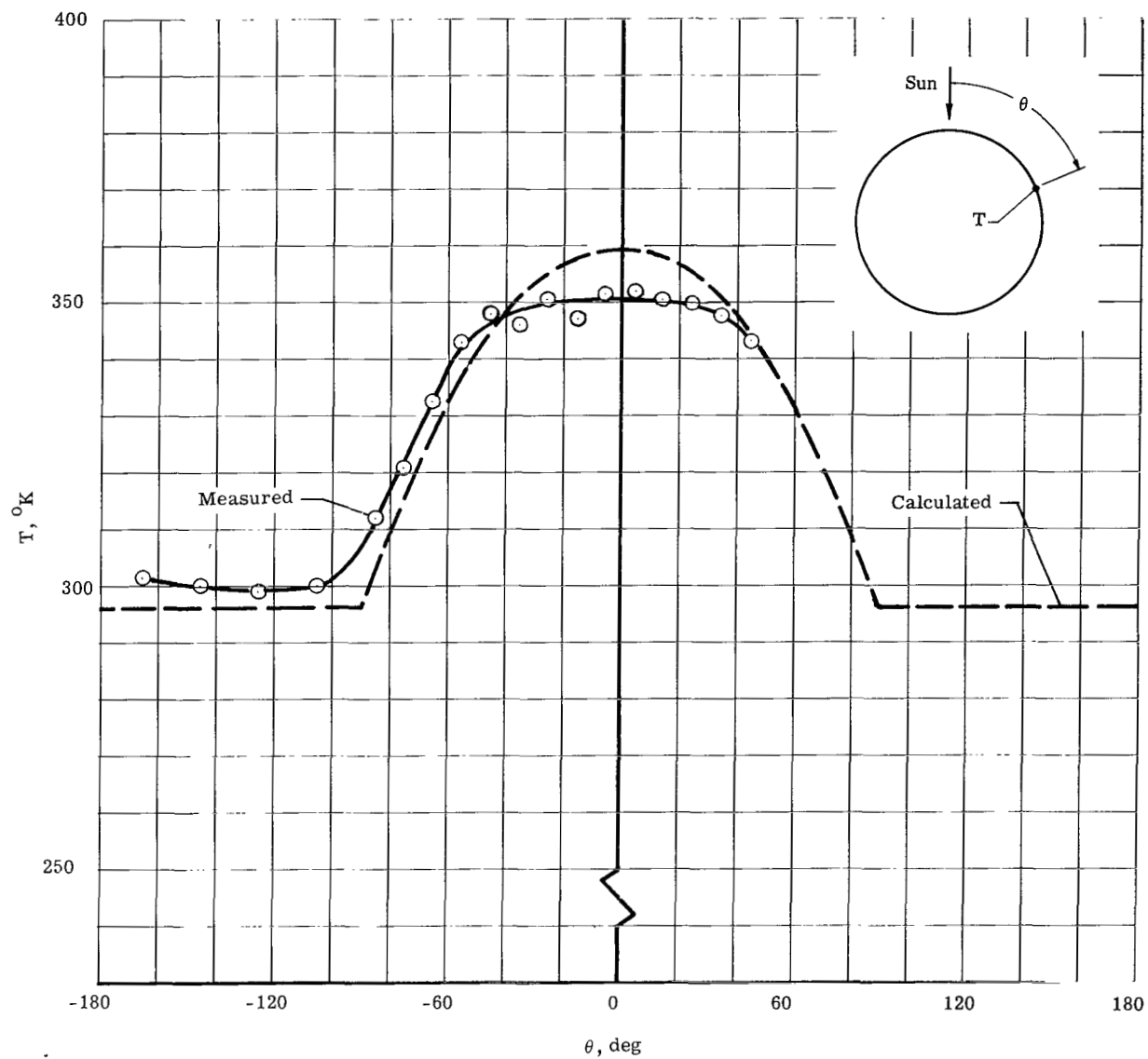
(a) Echo II model.

Figure 19.- Comparison of measured and calculated skin temperatures.
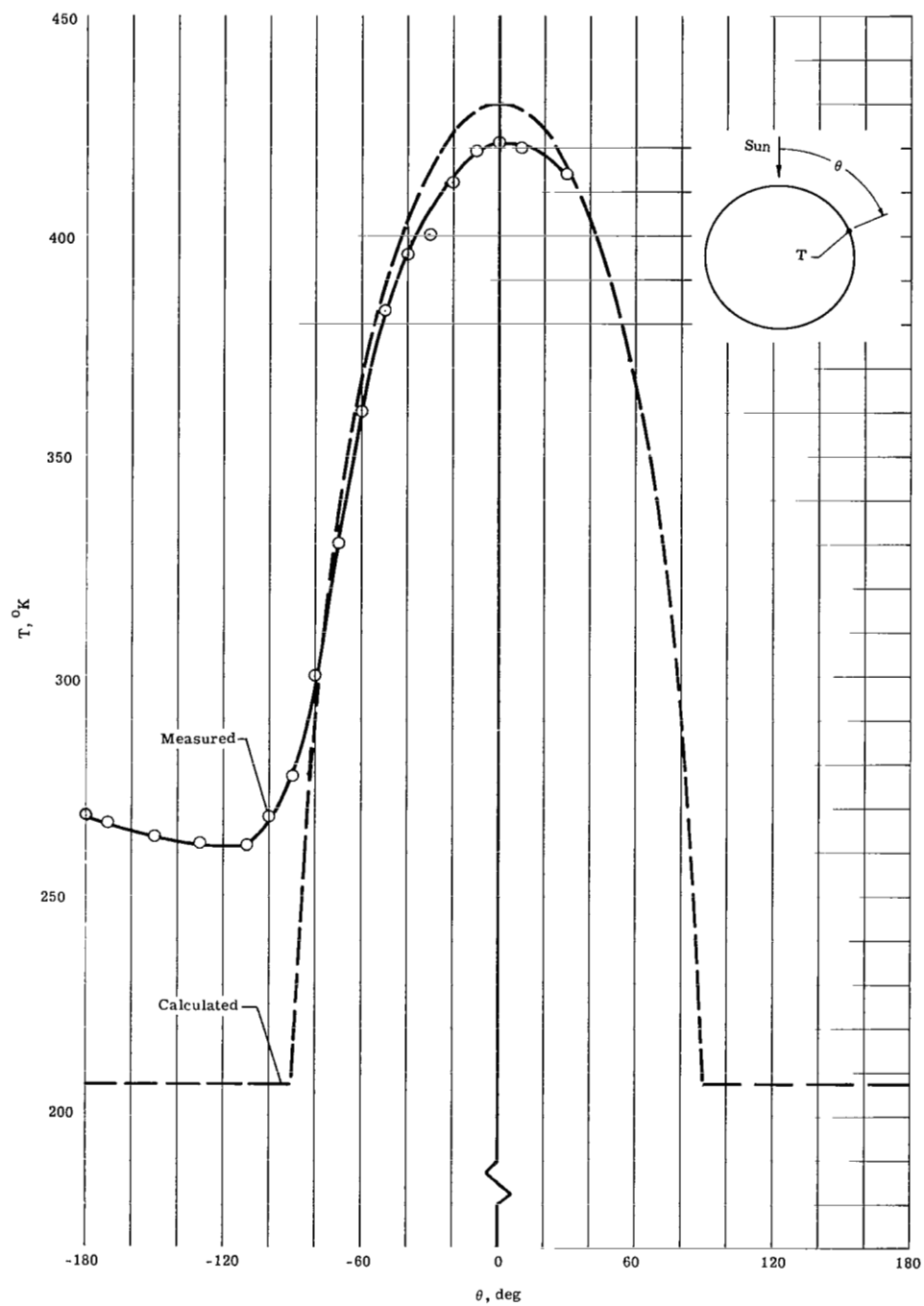
(b) Modified Echo II model.

Figure 19.- Continued.
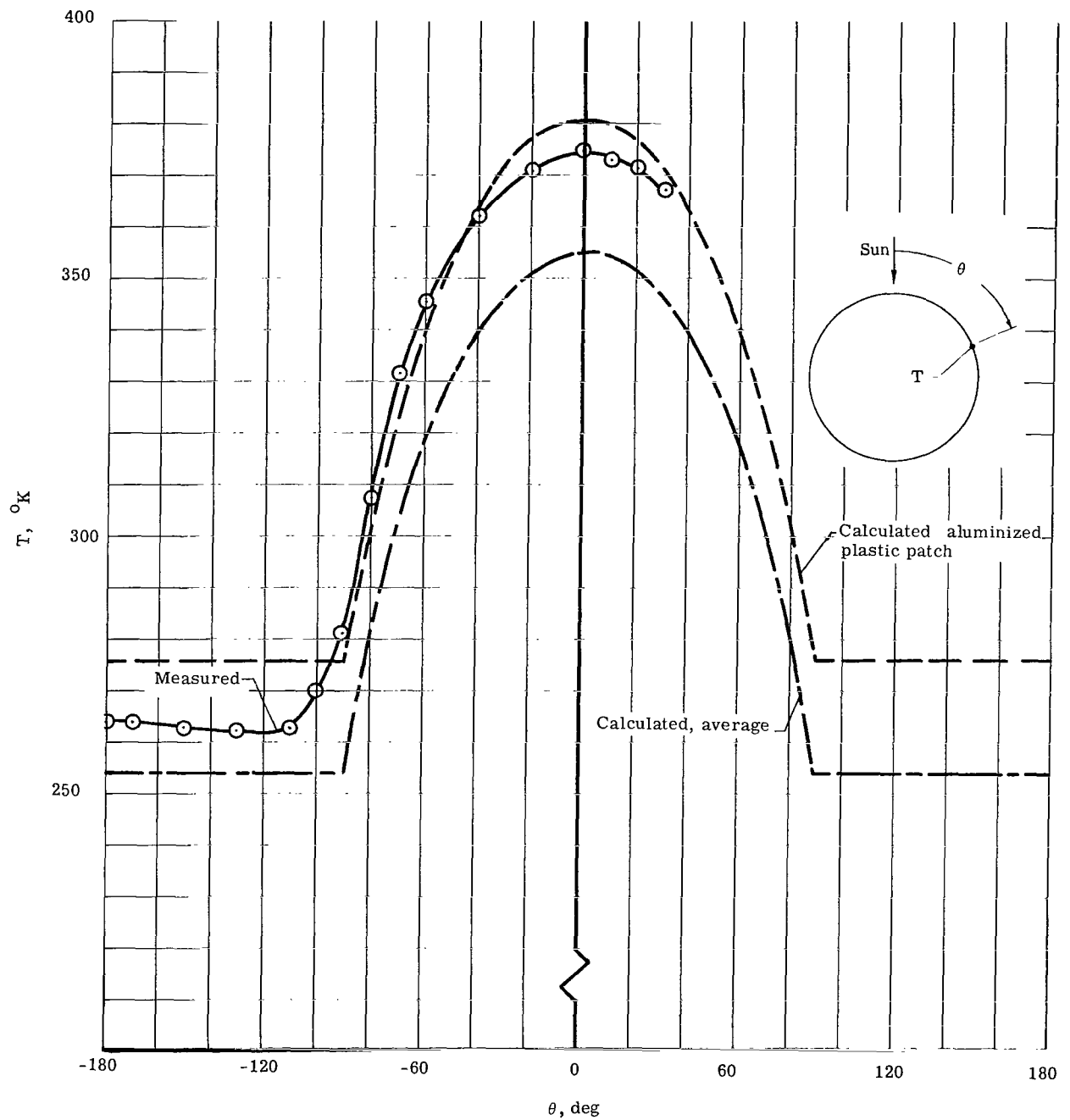
(c) Polka-dot balloon.

Figure 19.- Concluded.
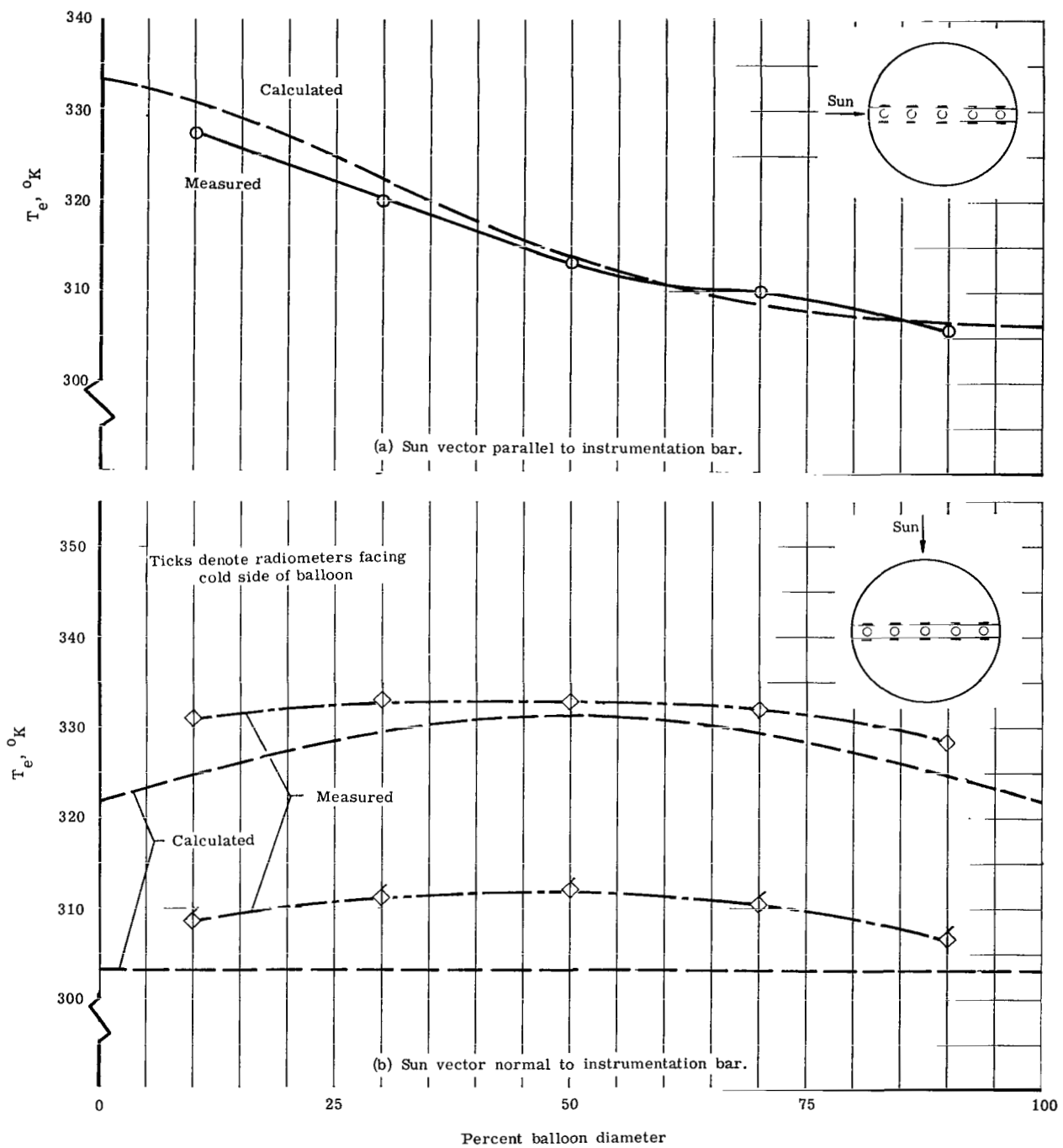
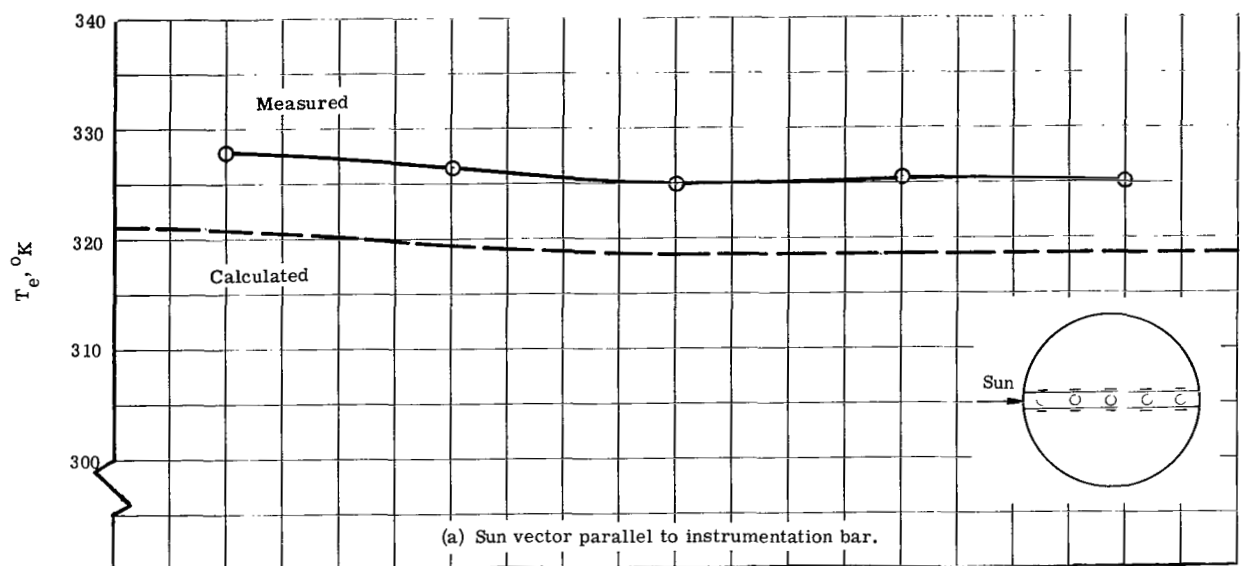Figure 20.- Comparison of measured and calculated internal irradiances for Echo II model.
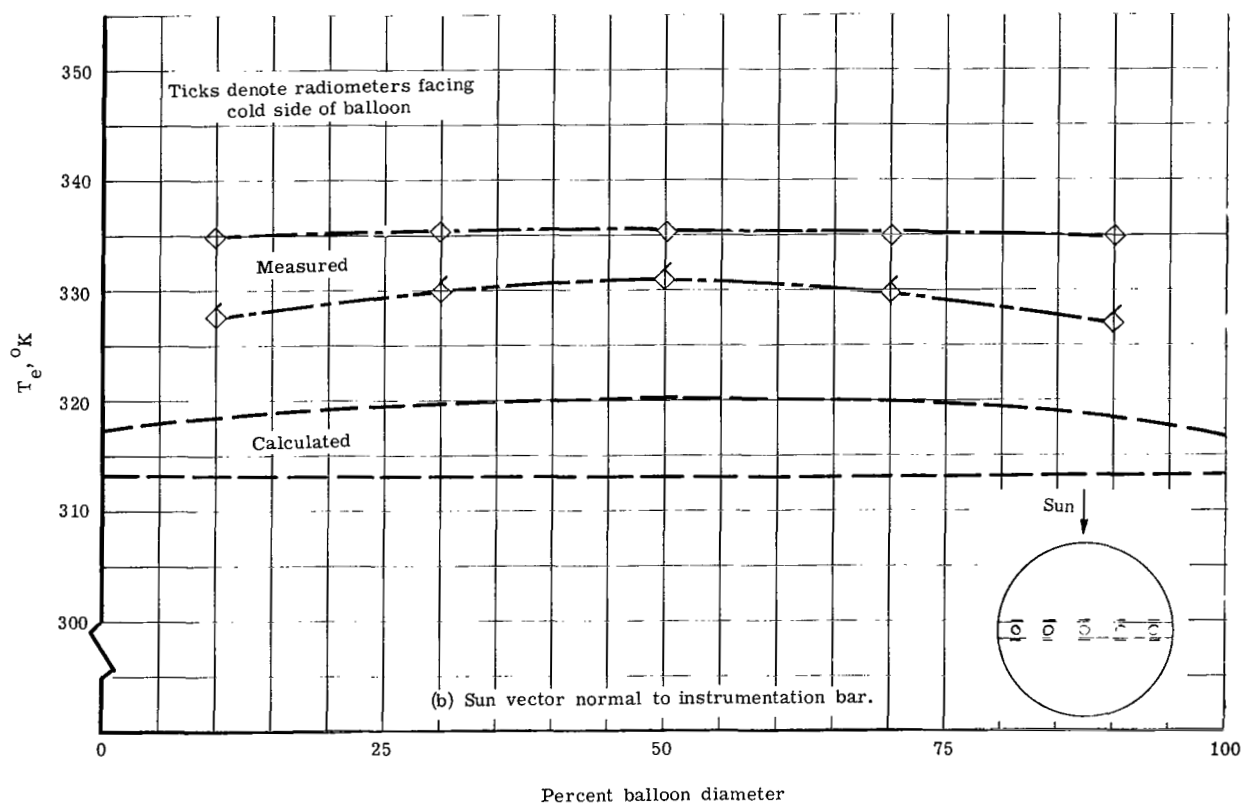
Figure 21.- Comparison of measured and calculated internal irradiances
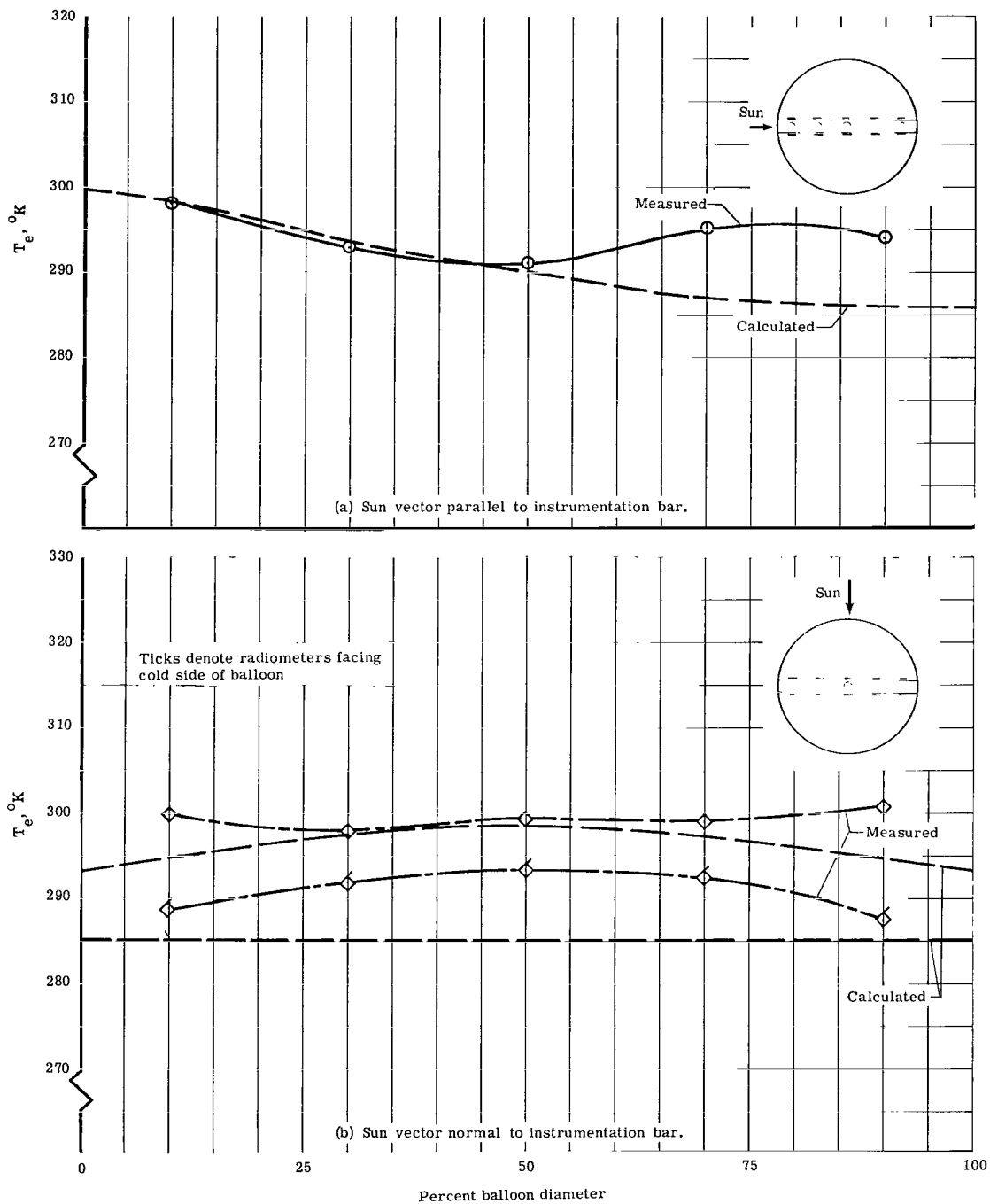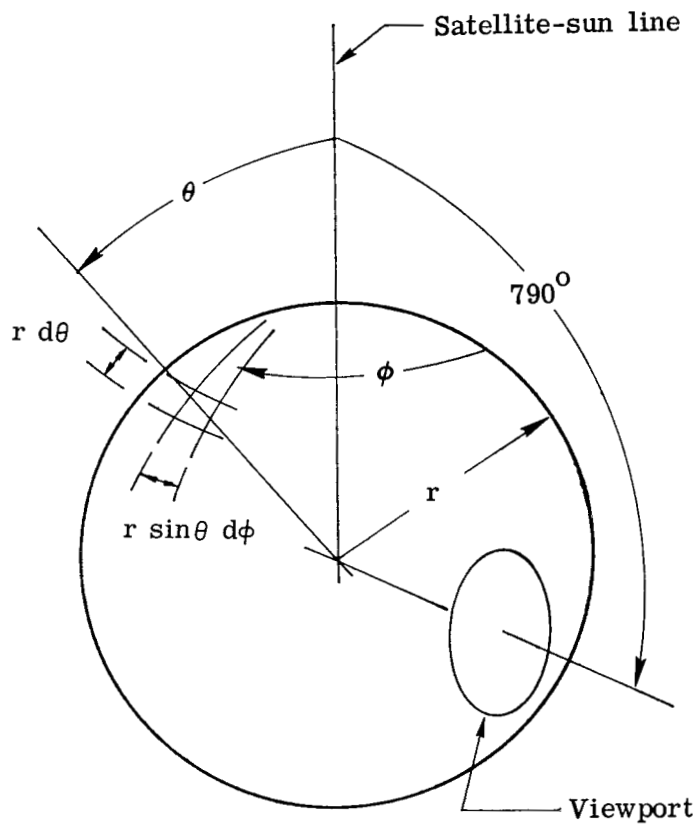for modified Echo II model.

(a) Sun vector parallel to instrumentation bar.

(b) Sun vector normal to instrumentation bar.

Percent balloon diameter

Figure 22.- Comparison of measured and calculated internal irradiances
for polka-dot model.

Figure 23.- Notation used to describe location of
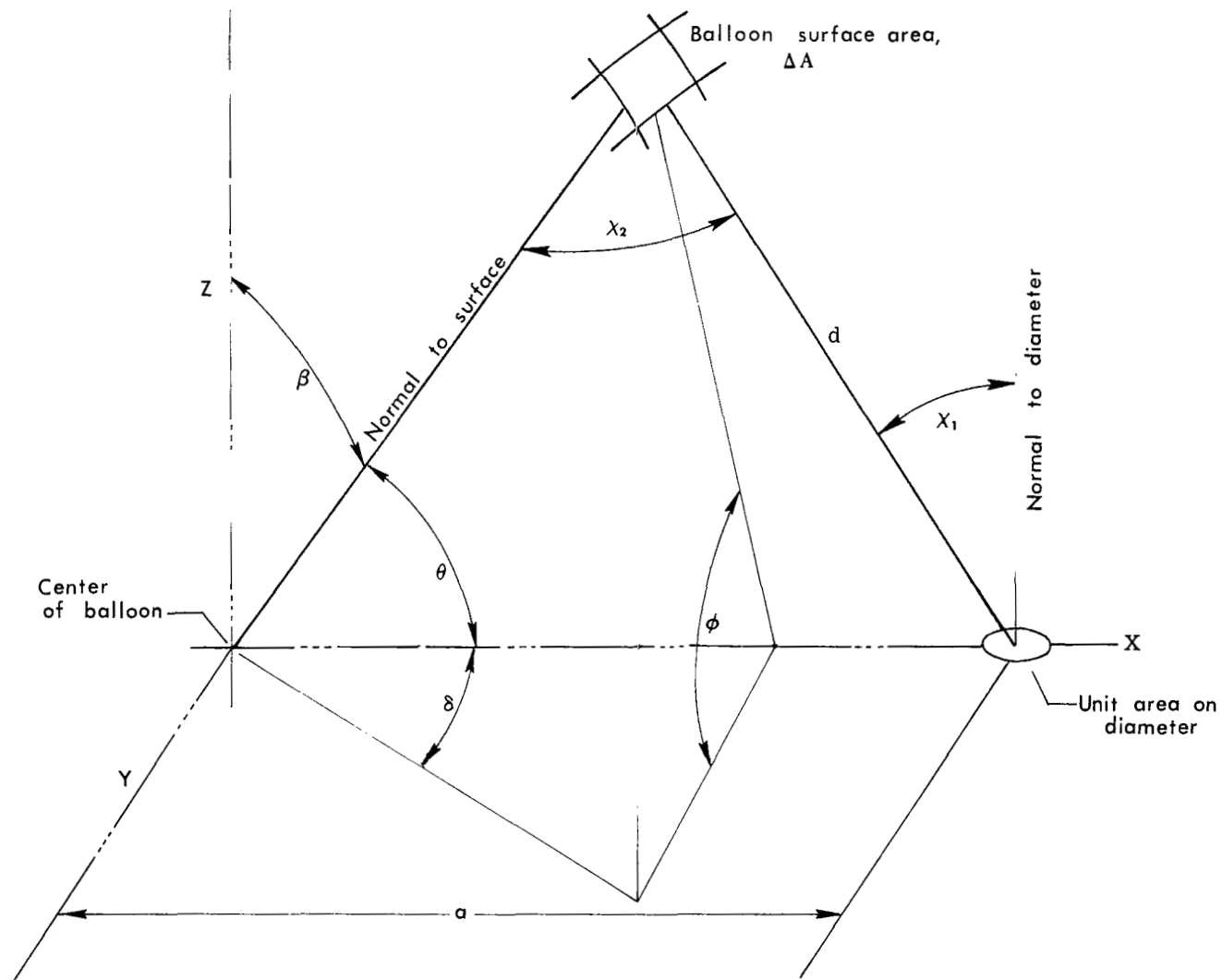balloon element with respect to sun.

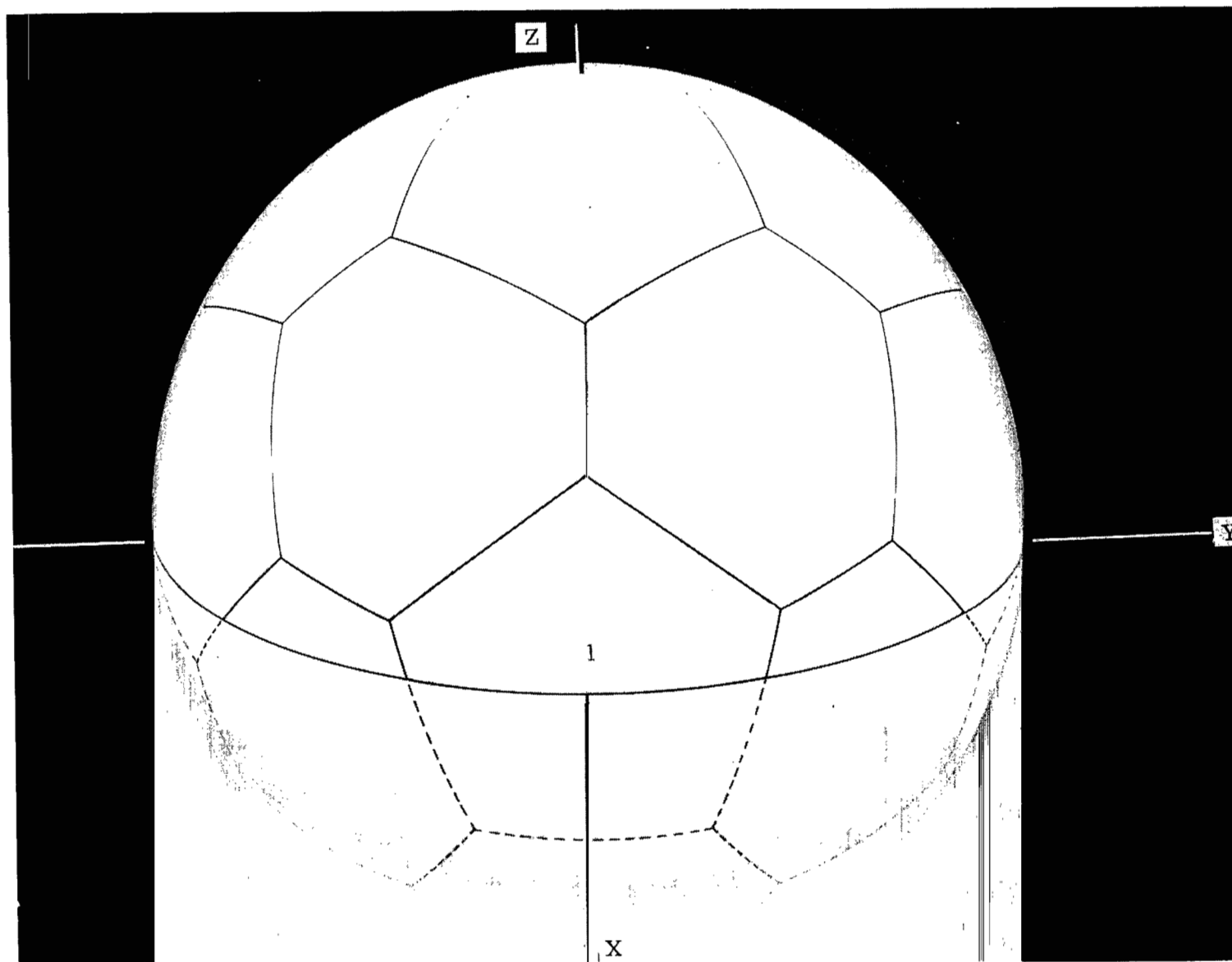Figure 24.- Notation used to describe geometry between balloon area ΔA and a unit surface on reference diameter.

Figure 25.- Layout of areas ΔA on a spherical surface.

L-68-9908.1